JOURNAL OF PETROLOGY | VOLUME 43 | NUMBER 6 | PAGES 1049–1087 | 2002

The Sulfide Capacity and the Sulfur Content at Sulfide Saturation of Silicate Melts at 1400°C and 1 bar

HUGH ST. C. O'NEILL[1]* AND JOHN A. MAVROGENES[1,2]

[1]RESEARCH SCHOOL OF EARTH SCIENCES, AUSTRALIAN NATIONAL UNIVERSITY, CANBERRA, ACT 0200, AUSTRALIA
[2]DEPARTMENT OF GEOLOGY, AUSTRALIAN NATIONAL UNIVERSITY, CANBERRA, ACT 0200, AUSTRALIA

RECEIVED AUGUST 15, 2001; REVISED TYPESCRIPT ACCEPTED JANUARY 9, 2002

The solubility of sulfur as S^{2-} has been experimentally determined for 19 silicate melt compositions in the system CaO–MgO–Al_2O_3–SiO_2(CMAS) ± TiO_2 ± FeO, at 1400°C and 1 bar, using CO–CO_2–SO_2 gas mixtures to vary oxygen fugacity (fO_2) and sulfur fugacity (fS_2). For all compositions, the S solubility is confirmed to be proportional to $(fS_2/fO_2)^{1/2}$, allowing the definition of the sulfide capacity (C_S) of a silicate melt as $C_S = [S](fO_2/fS_2)^{1/2}$. Additional experiments covering over 150 melt compositions, including some with Na and K, were then used to determine C_S as a function of melt composition at 1400°C. The results were fitted to the equation $C_S = A_0 + \sum_M A_M X_M + B_{Fe\text{-}Ti} X_{Fe} X_{Ti}$, *where* $A_{Fe} \gg A_{Ca} > A_{Mg}, A_{Na/K}, A_{Ti}$. *The FeO content of natural basalts is the dominant control on C_S. The equation for C_S was then combined with the equation for the thermodynamic equilibrium between silicate melt and immiscible FeS-rich sulfide melt, to develop an expression for the sulfur content at sulfide saturation (SCSS) of the silicate melt. The value of SCSS is independent of fO_2 and fS_2, but shows an asymmetric U-shaped dependence on the FeO content of the silicate melt. Many of the experiments on Fe-containing melt compositions were saturated with immiscible FeS melt, and these experiments were used to calibrate quantitatively SCSS at 1400°C as a function of melt composition.*

KEY WORDS: *sulfur; sulfide capacity; silicate melts; thermodynamics*

INTRODUCTION

Quantitative knowledge of the solubility of sulfur in silicate melts is fundamental to an understanding of many geological processes, such as: the origin of magmatic sulfide ores; sulfur degassing from volcanic eruptions and hence global climate change; the geochemical behaviour of the chalcophile trace elements, including the platinum group elements and the Re–Os isotopic system, and their use as tracers of core–mantle and crust–mantle differentiation in the Earth. The solubility of sulfur in silicate slags is also an important topic in extractive metallurgy, and has been much studied in this context, both theoretically and experimentally. In a classic paper, Fincham & Richardson (1954) proposed that at low fO_2 [more reducing than that defined by the quartz–fayalite–magnetite equilibrium (QFM)], sulfur dissolves in silicate melts as S^{2-}, and does so by replacing O^{2-} on the anion sublattice:

$$S^{2-} + \tfrac{1}{2}O_2 = O^{2-} + \tfrac{1}{2}S_2. \quad (1)$$

Because the number of O atoms in silicate melts greatly exceeds the number of other potential anions including S^{2-}, the concentration of O^{2-} is assumed to be constant. Reaction (1) therefore suggests the relationship

$$\ln C_S = \ln [S] + \tfrac{1}{2}\ln(fO_2/fS_2) \quad (2)$$

where [S] is the sulfide content of the melt (conveniently, in parts per million), and C_S is the 'sulfide capacity' of the melt, which may be thought of as analogous to an equilibrium constant for reaction (1). C_S is therefore a function of temperature (T) and pressure (P), and also of melt composition. Fincham & Richardson (1954) experimentally verified this relationship for silicate melts in

*Corresponding author. Telephone: +61 2 6125 5159. Fax: +61 2 6125 5989. E-mail: hugh.oneill@anu.edu.au

the system $CaO–Al_2O_3–SiO_2$ by holding slag compositions constant while varying fO_2 and fS_2 independently at atmospheric pressure. So influential was this study that subsequent experimental studies reported in the metallurgical literature, aimed at expanding the range of silicate slag compositions studied, have usually assumed the universality of the Fincham–Richardson relationship, rather than actually testing it. The experimental studies in the metallurgical literature have been reviewed comprehensively by Young *et al.* (1992) to *c.* 1990, but the field is still active, and more recent work has been reported by Seo & Kim (1999). These references show that all the silicate slag compositions studied by the metallurgists are far removed from natural silicate melt compositions, and it is not clear to what extent the metallurgical results can be applied to geologically relevant compositions.

Obviously C_S only has meaning if the concentration of sulfur (as S^{2-}) in a silicate melt is proportional to $(fS_2/fO_2)^{0·5}$ as postulated by Fincham & Richardson (1954). Although this relationship has been confirmed for a Hawaiian tholeiite composition by Katsura & Nagashima (1974) as a function of fO_2, and for a komatiitic composition by Shima & Naldrett (1975) as a function of fS_2, other studies (Haughton *et al.*, 1974; Buchanan & Nolan, 1979; Buchanan *et al.*, 1983) have shown deviations from the relationship. If real, these deviations require reanalysis of sulfide solubility theory as developed by the metallurgists. In fact, an attempt to account for S solubilities over a wide range of melt compositions including geologically relevant compositions has led to the development of a complicated theoretical model that is not based on the Fincham–Richardson relation (Poulson & Ohmoto, 1990). By contrast, Li & Naldrett (1993) considered only geologically relevant compositions and concluded that the solubility of S^{2-} in these melts depended only on the activity of their FeO component.

We have experimentally studied sulfur solubilities in silicate melts under controlled fO_2 and fS_2, first to test the $(fS_2/fO_2)^{0·5}$ relationship over a wide range of silicate melt compositions, and hence, if the relationship is confirmed, to determine the compositional dependence of C_S. We then use these data to develop a model to describe the sulfur content at sulfide saturation (SCSS) of silicate melts as a function of composition.

We have used the 'wire loop' technique, in which a small amount ($\sim$50 mg) of silicate melt is held on a loop of metal wire or ribbon by surface tension, and suspended in a gas mixing furnace, with fO_2 and fS_2 controlled using CO_2, CO and SO_2 as input gases. The experiments reported here have been undertaken at the relatively high T of 1400°C, to access a wide range of silicate melt compositions. Although even higher temperatures would have permitted the investigation of more MgO-rich compositions, such compositions typically cannot be quenched to glasses, causing potential analytical difficulties. Future work will address the important question of the temperature dependence of the sulfide capacity, and will also extend the study to oxidizing conditions where S dissolves in silicate melts as sulfate (SO_4^{2-}) rather than sulfide (S^{2-}). Previously published work (Mavrogenes & O'Neill, 1999) reported the effect of pressure on SCSS.

EXPERIMENTAL METHODS

Experimental procedures

Starting compositions were prepared from dried oxides and carbonates, mixed under acetone and then sintered at 1100°C. Small amounts of these mixes were made into a slurry using polyethylene oxide. The slurries were mounted on wire loops, and converted into glass beads by lowering into a furnace at $\sim$1400°C. The resulting beads were typically about 3 mm in diameter. Several of these wire loops plus beads could be hung in the furnace in a single experiment, by suspending the loops from a ring made of 0·5 mm Pt–Rh wire; typically, six or seven loops were used in most experiments.

Pt wire was used for mounting the Fe-free compositions. A few early experiments on Fe-bearing compositions mounted on Pt resulted in massive Fe loss to the Pt, as expected given the low fO_2 used in this study (e.g. Sugawara, 1999). The Fe-loss problem was solved by using Re ribbon (99·9% pure), which is commercially available as filament material for thermal ionization mass spectrometry. Fe loss to Re is almost negligible (Borisov & Jones, 1999), even when an immiscible FeS-rich sulfide melt develops during the experiment. The FeS melts seem to wet the Re ribbon, and are invariably found in the quenched run products as layers between Re ribbon and the silicate glass; but despite this intimate contact between Re and FeS, the observed solubility of Re in FeS is small (generally <0·2 wt %).

We also report a few experiments on $Fe_{20}–Ir_{80}$ alloy loops. These work fairly well, but are inconvenient in that the FeO content of the silicate melt in equilibrium with an alloy of given composition is fixed by fO_2. A different alloy composition is thus needed for each combination of FeO content and fO_2. Making Fe–Ir alloys and loops is an arduous business, so this approach was abandoned in favour of Re loops.

Experiments were performed in a vertical muffle tube furnace equipped for gas mixing. Both fO_2 and fS_2 were controlled independently using $CO_2–CO–SO_2$ gas mixtures, supplied to the furnace in accurately measured flow rates using Tylan F2800 mass flow controllers. Two controllers were available for each gas, with ranges 10 and 200 SCCM (standard cubic centimetres per minute) for CO and CO_2, and 10 and 100 SCCM for SO_2. The availability of two mass-flow controllers allows accurate

control of gas mixtures to fairly extreme mixing ratios. The direction of flow was in at the bottom of the furnace and out at the top, as is conventional for this type of experiment (see Darken & Gurry, 1946). Values of fO_2 and fS_2 from the gas mixes were calculated using thermodynamic data for gas species in the NIST-JANAF tables (Chase, 1998), by free energy minimization. For this calculation, we considered the species CO, CO_2, COS, SO_2, SO_3, S, S_2, S_3, S_4, S_6, S_8, CS, CS_2, and O_2, although only CO, CO_2, COS, and S_2 are calculated to be present in significant amounts at equilibrium for the mixtures used here. We checked our calculation routine against similar calculations reported in the studies of Haughton *et al.* (1974) and Buchanan & Nolan (1979). There is complete agreement between our calculations and those of the earlier studies.

Samples were introduced into the furnace at 600°C, which is a low enough T that they do not stick to each other or to the muffle tube if they happen to touch. The CO and CO_2 gases appropriate to the final gas mixture were then switched on, and the furnace was heated at 6°C/min to 1400°C. The SO_2 gas was added to the mixture when this T was reached.

We found that the performance of yttria-doped zirconia oxygen sensors ($SIRO_2$) degraded rapidly in an S_2-rich atmosphere at 1400°C. Consequently, oxygen sensors were employed only at intervals during this experimental campaign, as additional checks on the performance of the CO and CO_2 mass flow controllers. These tests were carried out at 1200°C. Sensors were not used during the actual experiments employing S-bearing gases.

At the end of the run, samples were quenched by dropping into water. They were mounted in epoxy and polished for analysis by electron microprobe.

Electron microprobe analysis

Each individual glass was analysed by combined wavelength- and energy-dispersive spectrometry (WDS and EDS, respectively) on the Cameca Camebax electron microprobe (EMP) at the Research School of Earth Sciences, ANU. Four separate EDS analyses provided a mean (and standard deviation) for each glass, which was used to calculate a ZAF correction coefficient. At 15 kV, each spectrum contained >600 000 counts.

WDS analyses for S were performed at 25 kV and 50–60 nA with a PET crystal. An analytical procedure was developed for analysis of samples with variable S^{2-}/SO_4^{2-}, whereby the combined sulfide plus sulfate peak was accurately measured for total dissolved sulfur. The sulfide and sulfate peak positions (located on FeS and $CaSO_4$ standards, respectively) were measured for 100 s, and backgrounds on each side of the combined peak were measured for 50 s each. A defocused 5 μm beam was used. At least 10 replicate analyses were performed on each sample to check for variability, to constrain the analytical error, and to lower the S detection limit. Each analysis took 5 min. Thus each sample took ~1 h to analyse. Detection limits were ~15 ppm S. During each analytical session, NBS 610 was used as a secondary standard. Ten to 15 spot analyses were made on the NBS 610 glass, and the C s^{-1} A^{-1} were adjusted to obtain a total of 580 ppm S. The standard deviations of the NBS 610 analyses were generally around 3–5%.

Our calibration was checked on VG2 (Jarosewich *et al.*, 1979), a natural glass used by several other workers for this purpose. We obtained 1403 ± 31 ppm, which is in excellent agreement with the previous determinations by EMP analysis (all in ppm, uncertainties 1 SD): 1340 ± 80 (Dixon *et al.*, 1991); 1420 ± 40 (Wallace & Carmichael, 1992); 1400 (Nilsson & Peach, 1993); 1365 ± 29 (Thordarson *et al.*, 1996); 1450 ± 30 (Métrich *et al.*, 1999); 1416 ± 36 (De Hoog *et al.*, 2001). In addition, Wallace & Carmichael (1992) reported 1320 ± 50 ppm from wet-chemical analysis. Available evidence for Fe^{2+}/Fe^{3+} of silicate melts (e.g. Kilinc *et al.*, 1983) indicates that Fe^{2+} should make up >95% of the total Fe in the silicate melts under the conditions of this study. We have therefore treated all Fe as Fe^{2+}.

Equilibration times

The time needed to achieve steady-state S contents (hence by inference, equilibrium) in Fe-free CMAS compositions was investigated by running the 'CMAS-7' compositions for different times, from 1 h to 50 h. Results are summarized in Fig. 1. Times are taken from when the gas mixture was switched on (furnace reached 1400°C). There should be zero S in all compositions at zero time. All subsequent Fe-free compositions were run for longer than 8 h (mostly ~16 h).

These Fe-free CMAS compositions are envisaged to approach equilibrium by the simple one-stage process of exchange of S for O [e.g. reaction (1)]. By contrast, equilibration of the Fe-containing samples also requires the reduction of Fe^{3+} in the starting material to Fe^{2+}, to establish the equilibrium Fe^{2+}/Fe^{3+} appropriate for the fO_2 of the run. Furthermore, for those runs that produced an immiscible sulfide liquid, segregation of this liquid [according to reaction (3), see below] also needs to take place. These reactions presumably take place sequentially rather than concurrently, as it is first necessary to establish the equilibrium Fe^{2+}/Fe^{3+} and build up S in the silicate before segregation of an immiscible sulfide liquid can occur. From this perspective, it could be anticipated that equilibrium in the Fe-bearing compositions would take longer to reach than in the CMAS compositions. Against this, Fe-bearing compositions are usually less viscous than

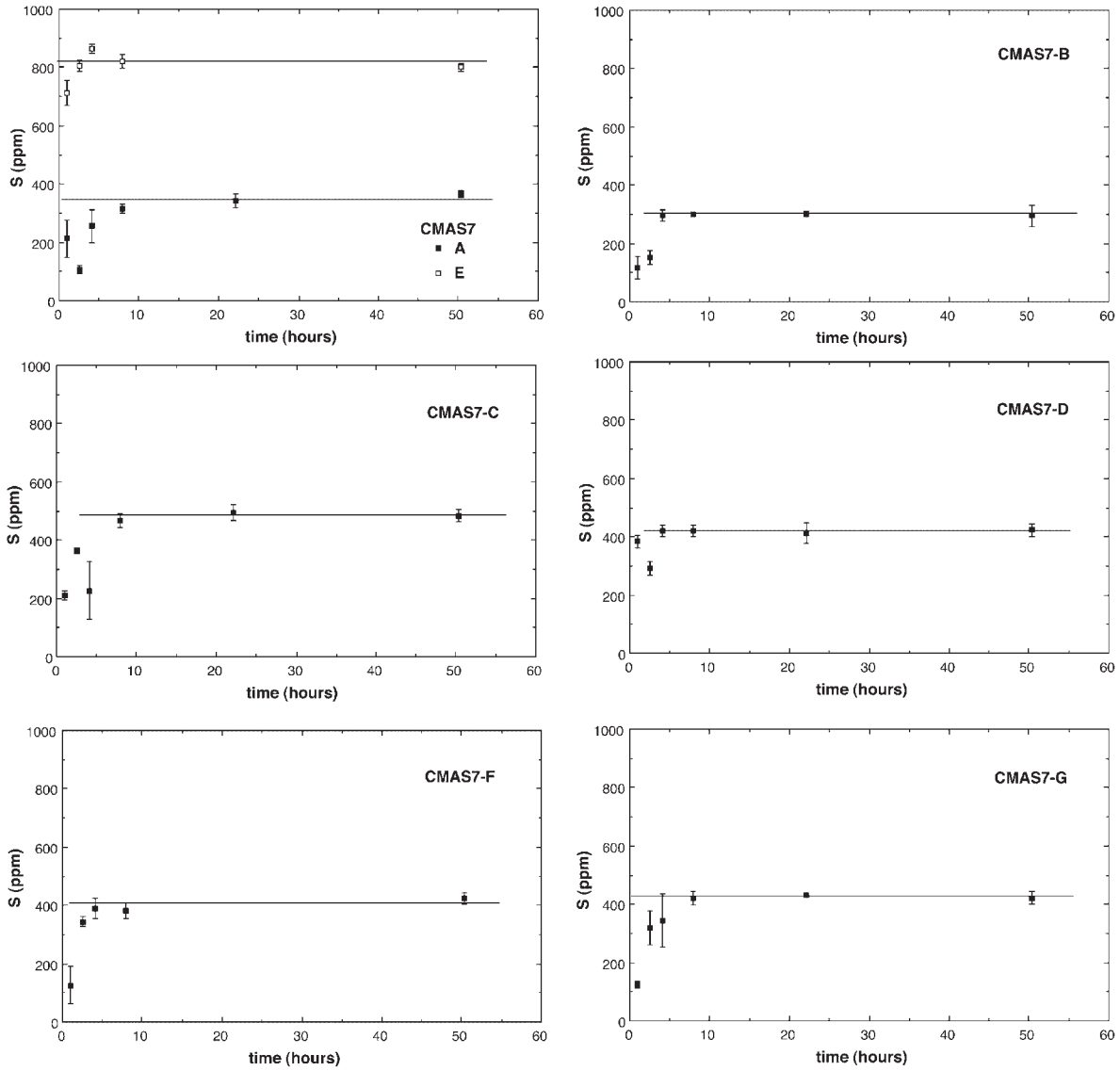

Fig. 1. Time series showing the time needed for sulfur solubilities of Fe-free silicate melts (CMAS7—see Table 1 for compositions) to reach steady-state values (hence, by inference, equilibrium). The time needed is ~8 h. It should be noted that the approach to steady state does not follow a smooth curve with time, probably because sample geometry was not controlled.

the CMAS compositions, and appear to have different wetting characteristics. Rather than form nearly spherical beads, many of the Fe-bearing samples appear to have crept along their Re ribbon, which gives these samples a different aspect ratio with greater surface area to volume, more favourable for equilibration with the gas. In fact, for the Fe-bearing compositions, the results (Fig. 2) show that a constant value of dissolved S was achieved even in the shortest time attempted (4 h), for both FeS-saturated and FeS-undersaturated conditions. An additional feature of the time series shown in Fig. 2 is the effectiveness of Re in minimizing Fe loss to almost negligible levels.

Experimental uncertainties

A priori knowledge of experimental uncertainties is required to judge whether the model used to fit the data is adequate. The accuracy of most of the results reported here depends almost entirely on three experimental variables: fO_2, fS_2 and the EMP analyses for S. The accuracy with which FeO is determined also becomes significant for high-FeO samples because of the very strong dependence of S solubilities on FeO content. Temperature is not a significant experimental uncertainty. All uncertainties reported in this paper are 1 SD.

The accuracy of reported fO_2 and fS_2 values depends on the input gas mixture (see Table 3, below). The

Table 1: Fe-free silicate melts used to investigate sulfur solubilities as a function of fO_2 and fS_2 (see Table 2)

Melt	CaO	MgO	Al_2O_3	SiO_2	$\ln(C_S)$*	χ^2_ν†
AD6						
AD eutectic	24·5(4)	10·2(2)	15·0(2)	50·3(4)	−2·44(3)	2·00
AD + Fo (15%)	21·2(1)	16·4(2)	12·7(1)	49·7(3)	−2·37(4)	2·00
AD + En (60%)	15·1(3)	20·8(2)	9·1(1)	54·9(3)	−2·71(4)	1·05
AD + Wo (140%)	39·6(6)	4·0(1)	6·1(2)	50·9(3)	−1·74(3)	1·05
AD + Qz (50%)	16·4(1)	6·6(1)	9·9(1)	66·8(2)	−3·46(5)	1·36
AD + TiO_2 (25%)	19·6(2)	8·0(1)	11·8(1)	40·2(4)‡	−2·09(3)	1·47
CMAS7						
A (1 bar eutectic, 1240)	16·0(1)	11·8(1)	15·1(2)	56·7(2)	−2·96(3)	0·27
B (fo + pr-en, 1371)	8·6(1)	19·6(1)	13·7(1)	57·7(4)	−3·06(4)	0·49
C (fo + o-en, 1353)	16·1(1)	19·2(1)	6·3(1)	58·3(3)	−2·61(3)	0·49
D (fo + sp, 1358)	12·4(1)	17·9(1)	21·1(2)	48·3(3)	−2·74(4)	0·27
E	21·1(2)	18·7(2)	9·9(1)	50·1(3)	−2·08(3)	0·32
F (SiO_2 + di, 1330)	18·1(1)	13·2(1)	5·7(1)	62·8(3)	−2·78(4)	0·10
G (an + di + wo + SiO_2, 1129)	25·4(1)	2·2(1)	11·8(1)	60·1(4)	−2·75(4)	0·67

Mean values with standard deviations are from four electron microprobe analyses of each sample in Table 2, i.e. 40–50 analyses in total.
*C_S = [S (in ppm)].$(fO_2/fS_2)^{1/2}$. From least-squares regression of data in Table 2, assuming uncertainties (1 SD) of 5% in [S] or as observed, whichever is larger, and of 0·05 in log fO_2 and log fS_2.
†Reduced chi-squared from the regression.
‡Plus 19·9(4) wt % TiO_2.

accuracy of fS_2 decreases greatly as fS_2 decreases, because the proportion of SO_2 in the input gas mixture becomes very small. Also, fO_2 and fS_2 are not independent variables, but the degree to which the one depends on the other also varies with the particular input gas mixture. For each group of six or seven samples run together, the errors in fO_2 and fS_2 are obviously the same, i.e. should not be treated as independent, uncorrelated uncertainties. To simplify matters, we assume that the uncertainties in log fO_2 and log fS_2 for every sample are independent of each other, and were both $\pm 0{\cdot}05$ in the earlier experiments, but improved to $\pm 0{\cdot}03$ in later experiments. These uncertainties in fO_2 and fS_2 propagate through equation (2) to produce uncertainties in C_S of 8·1% and 4·9%, respectively.

Observed standard deviations from EMP analyses are given for each experiment in the tables of results. In relative terms, these uncertainties range from 100% as S contents approach the limit of detection ($\sim$15 ppm), down to $\sim$1% in many of the experiments with the highest S contents (that is, those with S >2000 ppm). However, these uncertainties do not include errors in the setting up of the calibration for S on the EMP. This procedure involves normalization of the C s^{-1} A^{-1} to the value of the S content that we have assumed for the NBS 610 glass standard (namely, 580 ppm); this value is determined to 3–5% in each session, which must be included in the analytical uncertainty. There is also the possibility of instrument drift during an analytical session. We have therefore taken the total non-systematic uncertainty in S analyses (1 SD) to be either 5%, or as observed, whichever is the larger.

RESULTS

Testing the Fincham–Richardson relationship: [S] $\propto (fS_2/fO_2)^{1/2}$

Twelve Fe-free compositions in the system CaO–MgO–Al_2O_3–SiO_2 (CMAS) plus one composition in the system CMAS–TiO_2 were selected to test thoroughly the Fincham–Richardson hypothesis over as wide a range of fO_2 and fS_2 as is possible using CO–CO_2–SO_2 gas mixtures. The compositions were selected to cover a wide compositional range while still being above the liquidus at 1400°C, and quenching to homogeneous glasses. They include both relatively low melting point compositions [eutectic or peritectic compositions, mostly estimated from Longhi (1987)], plus compositions based on the anorthite–diopside eutectic, to which were added the

Table 2: Sulfur contents of CMAS melts, in ppm

	AD6											
Run:	14/2/97	13/2/97	2/8/97	16/2/97	7/2/97	24/3/98	8/2/97	17/2/97	1/3/97	2/3/97	28/2/97	5/3/97
Time (h):	7	6·3	22·3	14	17	67	16·5	17	12·2	14	17	7
log fS_2:	−1·91	−1·91	−1·91	−1·91	−1·91	−1·91	−1·91	−1·91	−3·36	−2·84	−2·47	−1·59
log fO_2:	−6·78	−7·28	−8·09	−8·79	−9·60	−9·60	−10·28	−10·92	−10·28	−10·28	−10·28	−10·28
AD eu	31(18)	66(18)	139(18)	280(19)	642(17)	605(27)	1014(98)	2715(25)*	258(22)	501(17)	524(31)	1887(42)
AD + Fo	45(14)	49(21)	145(18)	—	666(24)	746(17)	1315(87)	3140(41)	264(29)	—	560(25)	2122(36)
AD + En	26(10)	—	117(24)	193(22)	497(16)	526(23)	936(56)	2131(19)	188(28)	358(27)	436(25)	1501(41)
AD + Qz	24(28)	6(23)	64(14)	46(15)	196(32)	264(18)	456(44)	935(76)	69(26)	133(30)	202(56)	733(129)
AD + Wo	50(14)	117(57)	240(12)	497(19)	1294(24)	1352(43)	2426(154)	5583(59)	492(30)	—	1109(39)	3987(44)
AD + TiO_2	51(17)	79(14)	192(18)	364(19)	894(19)	923(31)	1708(50)	3957(34)	343(39)	652(50)	775(23)	2668(29)

	CMAS7									
Run:	22/5/99	23/5/99	13/5/99	3/8/99	26/5/99	21/5/99	28/5/99	1/6/99	2/6/99	3/6/99
Time (h):	15·5	18	50·3	16/8	24	17·1	23·5	26	25·8	21·3
log fS_2:	−1·91	−1·91	−1·91	−1·91	1·91	−3·07	−3·36	−2·84	−2·47	−1·59
log fO_2:	−8·09	−8·79	−9·60	−10·28	−10·92	−7·60	−10·28	−10·28	−10·28	−10·28
A	59(12)	127(20)	366(13)	765(18)	1602(37)	4(12)	161(20)	282(20)	459(12)	1116(22)
B	—	140(20)	295(37)	691(14)	1426(89)	19(14)	144(11)	276(25)	389(12)	984(27)
C	81(12)	190(18)	484(22)	1115(32)	2262(35)	24(17)	231(19)	399(23)	664(12)	1538(43)
D	66(16)	178(18)	423(21)	995(52)	2031(83)	—	191(20)	356(10)	566(22)	1405(19)
E	145(21)	339(16)	801(14)	1923(32)	3888(59)	32(18)	393(19)	659(17)	1076(24)	2678(32)
F	—	162(25)	423(20)	932(31)	2063(75)	6(13)	178(15)	325(17)	525(29)	1340(28)
G	—	—	422(23)	862(41)	2007(25)	19(12)	204(18)	350(28)	568(23)	1416(18)

Values are means of 10–12 spot analyses, with the standard deviation in parentheses.
*This value is the mean of runs 10/7/99 and 16/8/99 (see Table 7). The AD eutectic sample in run 17/2/97 dropped off.

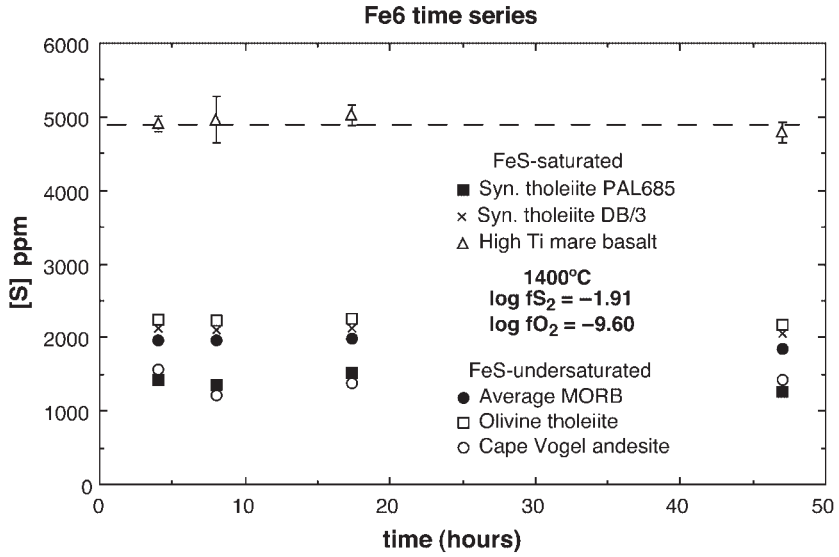

Fig. 2. Time series for 'Fe6' compositions on Re loops, all at $\log fO_2 = -9{\cdot}60$, $\log fS_2 = -1{\cdot}91$. At these conditions, three compositions are FeS undersaturated, and three compositions have exsolved some immiscible FeS melt. Regardless, all compositions appear to have reached the steady-state S solubility in the shortest run time, 4 h. The FeS-undersaturated compositions show a slight decrease in FeO from Fe loss to the Re at the longest run time (47 h), the most loss being 8% of the initial FeO. In the FeS-saturated compositions, the amount of FeO in the silicate melt is buffered, and Fe loss to the Re does not result in decreasing FeO content of the silicate melt. Error bars (2 SD) are shown for one composition only.

Table 3: Run conditions for 'Fe6' equilibration experiments at 1400°C

Run	CO (SCCM)	CO_2 (SCCM)	SO_2 (SCCM)	$\log fO_2$	$\log fS_2$	Time (h)
18/6/99	20·0	59·6	2·06	−7·60	−3·07	26·5
13/8/99	20·0	59·6	20·0	−7·28	−1·91	9
21/6/99	40·0	54·6	5·50	−8·09	−1·91	22
22/6/99	60·0	36·6	3·35	−8·79	−1·91	26
16/6/99	80·0	17·0	3·00	−9·60	−1·91	4
17/6/99	80·0	17·0	3·00	−9·60	−1·91	8
10/6/99	80·0	17·0	3·00	−9·60	−1·91	17·3
11/6/99	80·0	17·0	3·00	−9·60	−1·91	47
25/6/99	91·0	6·00	3·00	−10·27	−1·91	27
28/6/99	97·0	—	3·03	−10·92	−1·91	26
30/6/99	87·8	12·0	0·20	−10·27	−3·36	28·7
2/7/99	88·6	11·4	0·50	−10·27	−2·84	27
7/7/99	88·8	10·2	1·00	−10·27	−2·47	25·3
9/7/99	94·2	—	5·80	−10·27	−1·59	24·5

following components: SiO_2, $MgSiO_3$, $CaSiO_3$, Mg_2SiO_4, and TiO_2 in amounts close to the maximum possible at 1400°C. These compositions were run in two groups, one of six compositions (called AD6, where AD stands for anorthite–diopside) and the other of seven (CMAS7). The compositions are given in Table 1.

The low fO_2 limit of these experiments was determined by the O_2 content of the input gas mixture; we cannot produce conditions more reducing than are obtained with CO_2-free input mixtures (i.e. CO–SO_2 only). The high fO_2 or low fS_2 limits occur as the solubility of S approaches the analytical limit of detection, which is

$\sim$15 ppm. Also, the control of fS_2 at values of fS_2 $<10^{-3.5}$ bars becomes too imprecise to be useful, because the input flow rate of SO_2 is so low. The high fS_2 limit is defined by the experimental requirement for the input gas, $pCO_2 + pCO + pSO_2 = 1$ bar. Caution also dictates that fS_2 should not be too high lest condensing elemental S clogs up the gas outlet of the furnace. Nevertheless, within these limits, we can vary fO_2 by four orders of magnitude and fS_2 by nearly two orders of magnitude, while keeping the major-element composition of the silicate melt constant.

Experimental sulfur solubilities are given in Table 2, and are plotted as a function of fO_2 at constant fS_2 in Fig. 3a and b, and as a function of fS_2 at constant fO_2 in Fig. 4a and b. It may be seen that the solubility of S follows the Fincham–Richardson relationship completely. Statistical analysis of the data by least-squares regression is summarized in Table 1. It should be noted that the very low S contents in the experiments at the highest fO_2 values are consistent with negligible sulfate (SO_4^{2-}) or sulfite (SO_3^{2-}).

Six Fe-containing compositions were selected for a similar test. These compositions (called 'Fe6') were chosen in part to replicate previous experimental work (Table 3). Although approaching natural basaltic silicate melts, these compositions do not contain alkalis (Na or K) because these are lost by evaporation under the conditions of the experiment.

For Fe-bearing systems, the composition of the silicate melt cannot be kept constant over such wide ranges of fO_2 and fS_2, as FeO is lost from the silicate melt when the sulfide (FeS) saturation surface is reached. This happens as fO_2 is lowered or fS_2 raised, according to the reaction

$$\underset{\text{silicate melt}}{\text{FeO}} + \tfrac{1}{2}S_2 = \underset{\text{sulfide melt}}{\text{FeS}} + \tfrac{1}{2}O_2. \qquad (3)$$

Because of loss of FeO from the original starting compositions by this means (and by alloying of Fe with the Re wire, although this is minimal), full major-element analyses of all experiments are reported (Table 4). Results with no loss of Fe by FeS exsolution are plotted as a function of fO_2 in Fig. 5. Again, the data are in complete agreement with the Fincham–Richardson relationship [reaction (1)]. Although this result is not unexpected, other possibilities are conceptually possible. For example, the present results rule out significant solubility of molecular S. This contrasts with the solubility in silicate melts of other volatile components such as H_2O and CO_2, both of which dissolve not only as the anionic species OH^- and CO_3^{2-} but also as the molecular species H_2O and CO_2 (Kohn, 2000; Brooker *et al.*, 2001*a*, 2001*b*). The results from the iron-bearing compositions imply that only a component with FeS stoichiometry occurs, and not, for example, a component with pyrite stoichiometry (FeS_2). We find no evidence in our data for an Fe_3SO_2 component as postulated by Poulson & Ohmoto (1990) from modelling of previous experimental work. As will be discussed below, this may be because of errors in previous experimental work.

Once the actuality of the Fincham–Richardson relationship is taken as established, measuring S solubilities over a range of fO_2 and fS_2 becomes redundant. Instead, it suffices to choose just one experimentally convenient condition of fO_2 and fS_2 to explore further the influence of the major-element composition of the silicate melt on S solubility.

Effect of silicate melt composition—the FeO component

As noted above, the six FeO-containing compositions reach sulfide saturation at both the higher fS_2 and lower fO_2 conditions of this study. Precipitation of FeS then lowers the FeO content of the silicate melt, but all other components (i.e. CaO, MgO, Al_2O_3, SiO_2, TiO_2) are conserved, so that the resulting compositions lie on binaries between FeO and an Fe-free end-member composition in the system CMAS $\pm$ TiO_2. Similar binary joins arise in experiments that measure the activity of FeO ($a_{\text{FeO}}^{\text{silicate}}$) in silicate melts by equilibrating the melt with Fe metal under controlled fO_2. In such experiments, the FeO component in the melt increases as fO_2 is increased, according to the reaction

$$\underset{\text{metal}}{\text{Fe}} + \tfrac{1}{2}O_2 = \underset{\text{silicate melt}}{\text{FeO}}. \qquad (4)$$

Doyle & Naldrett (1986) and Doyle (1988, 1989), who undertook several series of experiments of this type, used the term 'Matrix' to describe the FeO-free end-members of their binary joins. The FeO-free end-member or 'Matrix' compositions of this study are given in Table 5.

The values of C_S, calculated from the sulfur solubilities in Table 4, are plotted against the FeO content of the melt for two of the binaries in Fig. 6. The data form a smooth curve, which is well described by a linear relationship between the logarithm of C_S and c_{FeO}. For a preliminary fitting of the data, we use the empirical relationship

$$\ln C_S = \ln C_S^{\circ}(1 - c_{\text{FeO}}/100) + B.c_{\text{FeO}}. \qquad (5)$$

The rationale for this relationship is that C_S° is the sulfide capacity of the FeO-free end-member or 'Matrix' component (i.e. for the FeO-free compositions as given in Table 5). A more complete equation that takes into account the dependence of C_S on all major-element oxide components will be introduced later (in the section 'Thermodynamic theory'), with more theoretical justification. The quality of the fits is demonstrated in Fig. 7a–f.

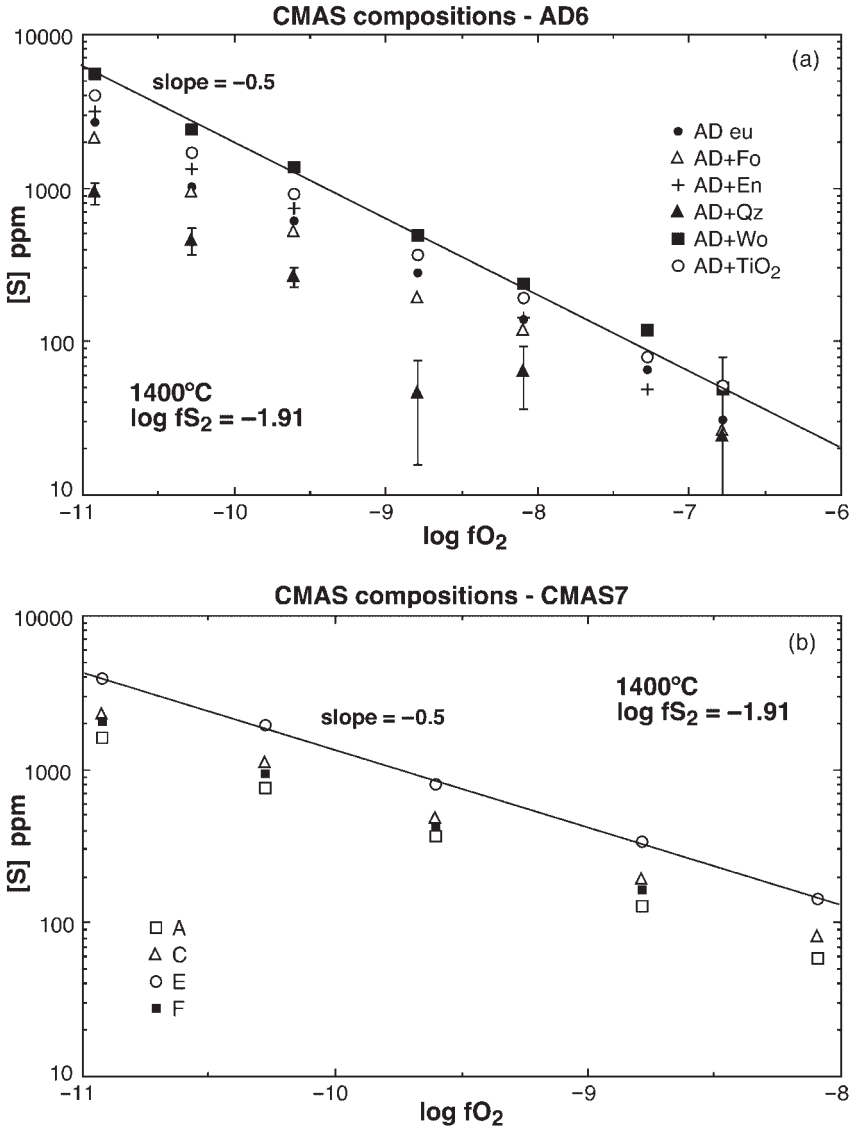

Fig. 3. S solubilities in Fe-free compositions as a function of fO_2 at constant fS_2 (log $fS_2 = -1{\cdot}91$). (a) AD6 compositions; (b) CMAS7 compositions (only four shown for clarity). The lines are not best fits to the data, but the theoretical slope of $-0{\cdot}5$, positioned arbitrarily for comparison with the data.

Examination of these plots, supported by the preliminary fitting, indicates that the value of the B parameter is the same in five of the six FeO–'Matrix' binaries, the exception being the high-Ti mare basalt. The value of the B parameter for the high-Ti mare basalt is $\sim$25% lower. The results of this fitting are given in Table 6.

As previous geologically oriented investigators have all noted, C_S greatly depends on the FeO content of the melt. This is not quite so apparent from the data in metallurgical literature, as these experimental studies are mainly concerned either with very low-FeO compositions, or with compositions near the FeO–SiO_2 binary [see, for example, studies listed by Young *et al.* (1992)]. As Fig. 6 shows, the exponential nature of the relationship between C_S and FeO means that the effect of FeO on C_S increases as FeO increases. Thus, at a few wt % FeO, the FeO content of the melt does not completely dominate C_S. On the other hand, for melts with more than $\sim$10 wt % FeO, the other components are more-or-less irrelevant; the total variation in the value of C_S° among the five 'terrestrial' compositions is only 0·01, which is equivalent to a change of 0·2 wt % FeO at 10 wt % FeO. This is close to the analytical error. It should be noted that a recent inter-laboratory comparison of some

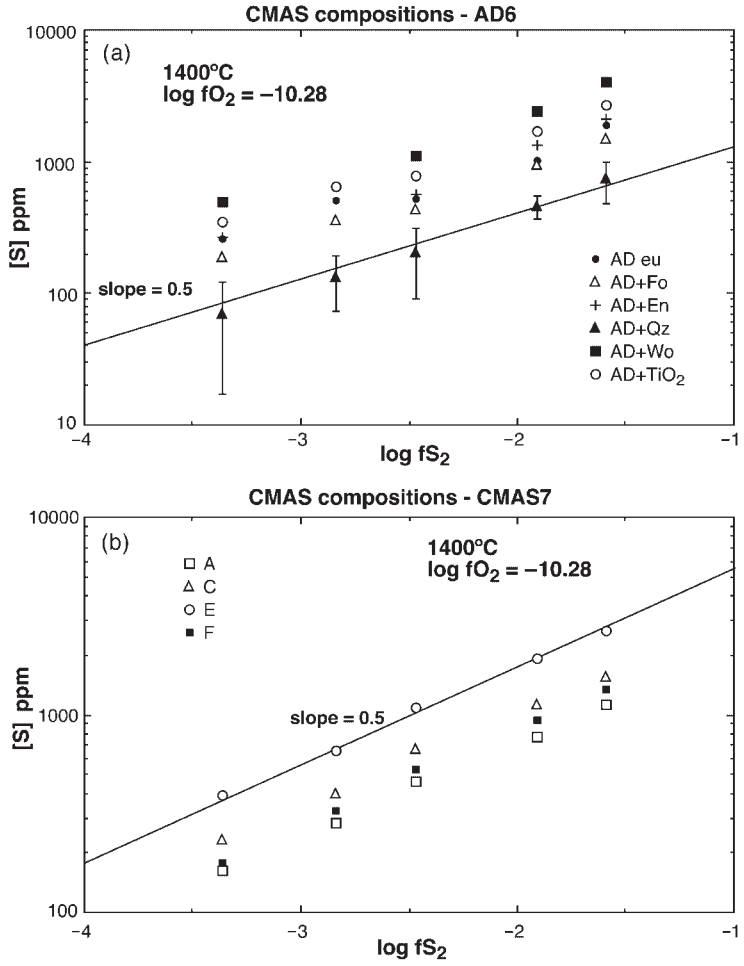

Fig. 4. S solubilities in Fe-free compositions as a function of fS_2 at constant fO_2 ($\log fO_2 = -10{\cdot}28$). (a) AD6 compositions; (b) CMAS7 compositions (only four shown for clarity). The lines are not best fits to the data, but show the theoretical slope of 0·5.

homogeneous glasses produced from natural compositions demonstrates differences in reported FeO contents of about this level (see Jochum *et al.*, 2000).

The dominant effect of FeO on C_S also means that FeO-rich compositions are not suitable for studying the dependence of C_S on other oxide components. Although this may seem of little practical importance for geological applications, it is important for understanding the fundamental thermodynamic basis for the effects of composition on C_S.

C_S in other FeO-free systems at 1400°C

Accordingly, we have made an extensive study of the compositional dependence of C_S in FeO-free systems to supplement the data in Table 2. Results are given in Tables 7–9, and are plotted in Figs 8–11. The general approach has been to start with the anorthite–diopside eutectic composition (ADeu) and add various components (SiO_2, Al_2O_3, TiO_2, $CaSiO_3$, Mg_2SiO_4, and $MgSiO_3$) to this composition. The binary between diopside and anorthite was also studied (Fig. 8). Relative to ADeu, TiO_2 and $CaSiO_3$ cause an increase of C_S, whereas Al_2O_3 and SiO_2 cause a decrease. In most cases, C_S changes approximately linearly with the added component, but where large amounts of the component can be added (e.g. $CaSiO_3$ and SiO_2), the relationship is clearly non-linear. As for FeO, these systems follow a logarithmic relationship between C_S and composition.

We also attempted to study the effects of alkali components (Na_2O and K_2O). Results are given in Table 10. The alkalis are volatile under the conditions of the experiment, hence composition changes continuously during the experiment and the extent to which equilibrium is achieved with respect to S solubility is uncertain. However, taking this into account, it nevertheless seems a robust conclusion that neither Na_2O nor K_2O causes a significant increase in C_S.

Table 4: Results of experiments on 'Fe6' melt compositions (see Table 3 for run conditions)

Run	SiO_2	TiO_2	Al_2O_3	FeO	MgO	CaO	S (ppm)
Synthetic tholeiite PAL 685							
18/6/99	59·8(2)	—	12·5(1)	14·7(2)	3·8(1)	8·8(1)	105(16)
13/8/99	59·0(3)	—	13·2(2)	14·9(1)	4·2(1)	9·0(1)	238(11)
21/6/99	60·1(5)	—	12·7(1)	14·8(1)	3·8(1)	8·9(1)	622(41)
22/6/99	59·4(1)	—	12·5(2)	14·5(2)	3·9(1)	8·9(2)	1342(28)
16/6/99	63·2(4)	—	13·3(1)	9·8(2)	4·0(1)	9·4(1)	1425(55)
17/6/99	63·7(1)	—	13·6(1)	9·7(1)	4·1(1)	9·4(1)	1345(22)
10/6/99	63·2(4)	—	13·4(1)	9·6(1)	4·0(1)	9·4(1)	1521(29)
11/6/99	63·7(1)	—	13·4(1)	8·8(1)	4·0(1)	9·5(1)	1262(39)
25/6/99	66·5(4)	—	14·2(1)	4·2(1)	4·2(1)	10·1(1)	921(41)
28/6/99	67·7(2)	—	15·0(2)	1·86(7)	4·6(1)	10·1(2)	960(25)
30/6/99	59·5(1)	—	13·2(1)	13·3(2)	4·2(1)	9·0(1)	1169(26)
2/7/99	61·8(3)	—	13·2(2)	11·9(2)	4·0(1)	9·2(1)	1580(36)
7/7/99	64·9(2)	—	13·8(1)	7·5(2)	4·1(1)	9·7(1)	1106(38)
9/7/99	66·9(2)	—	15·1(1)	2·99(5)	4·7(1)	10·3(1)	920(33)
Average MORB							
18/6/99	52·6(2)	1·4(1)	15·2(1)	10·2(3)	7·7(1)	12·4(1)	69(14)
13/8/99	52·4(1)	1·4(1)	16·1(1)	9·4(1)	8·0(1)	12·6(1)	134(10)
21/6/99	51·2(7)	1·3(1)	14·8(3)	10·0(1)	7·4(1)	12·1(2)	389(15)
22/6/99	52·6(2)	1·4(1)	15·2(1)	10·1(1)	7·7(1)	12·4(1)	828(27)
16/6/99	52·6(3)	1·3(1)	15·3(2)	10·2(2)	7·8(1)	12·4(1)	1964(68)
17/6/99	52·7(3)	1·3(1)	15·3(2)	10·2(1)	7·6(1)	12·4(1)	1964(19)
10/6/99	52·5(3)	1·3(1)	15·2(2)	10·2(1)	7·7(1)	12·4(2)	1995(54)
11/6/99	52·8(3)	1·3(1)	15·3(2)	9·4(2)	7·7(1)	12·5(2)	1856(27)
25/6/99	55·5(3)	1·4(1)	16·1(1)	5·2(2)	8·1(2)	13·3(1)	1625(34)
28/6/99	56·1(4)	1·4(1)	17·2(2)	2·5(2)	8·7(1)	13·5(1)	1883(44)
30/6/99	51·9(1)	1·3(1)	15·9(2)	9·7(2)	8·2(1)	12·5(1)	793(18)
2/7/99	52·9(4)	1·3(1)	15·4(2)	9·7(2)	7·9(1)	12·5(1)	1477(34)
7/7/99	53·7(1)	1·4(1)	15·5(1)	8·7(2)	7·9(1)	12·7(1)	1904(122)
9/7/99	55·3(2)	1·4(1)	16·9(1)	3·7(2)	8·7(1)	13·5(1)	1683(31)
Olivine tholeiite							
18/6/99	53·8(2)	2·3(1)	13·8(1)	12·2(1)	8·6(1)	9·3(1)	85(21)
13/8/99	53·2(2)	2·4(1)	14·6(1)	11·5(1)	8·9(1)	9·4(1)	166(19)
21/6/99							
22/6/99	54·1(2)	2·3(1)	13·8(2)	11·9(1)	8·5(1)	9·2(1)	972(46)
16/6/99	53·9(1)	2·3(1)	13·9(1)	11·7(2)	8·6(1)	9·3(1)	2126(29)
17/6/99	54·0(2)	2·3(1)	13·9(1)	11·7(1)	8·6(2)	9·3(1)	2121(26)
10/6/99	54·0(3)	2·3(1)	13·9(1)	11·4(1)	8·5(1)	9·3(1)	2220(77)
11/6/99	54·2(5)	2·3(1)	13·9(2)	11·3(1)	8·6(2)	9·4(1)	2181(29)
25/6/99	57·3(1)	2·4(1)	14·7(1)	5·6(1)	9·0(2)	9·9(1)	1588(139)
28/6/99	58·6(2)	2·5(1)	16·0(1)	2·6(1)	9·9(1)	10·2(1)	1639(34)
30/6/99	53·0(1)	2·2(1)	14·5(1)	11·5(1)	9·1(1)	9·3(1)	945(33)
2/7/99	54·1(2)	2·3(1)	13·9(1)	11·7(1)	8·6(1)	9·3(1)	1717(36)
7/7/99	55·7(1)	2·4(1)	14·3(1)	9·3(1)	8·9(1)	9·7(2)	1737(37)
9/7/99	57·6(4)	2·4(1)	15·7(2)	3·9(1)	9·8(2)	10·2(1)	1567(39)

Table 4: continued

Run	SiO_2	TiO_2	Al_2O_3	FeO	MgO	CaO	S (ppm)
Synthetic tholeiite DB/3							
18/6/99	49·8(2)	0·0	14·4(1)	16·8(1)	11·0(1)	8·5(1)	147(15)
13/8/99	49·5(4)	0·0	15·2(1)	15·5(2)	11·3(1)	8·6(1)	287(19)
21/6/99	49·7(1)	0·0	14·5(1)	16·7(1)	10·8(1)	8·5(1)	918(41)
22/6/99	49·9(3)	0·0	14·6(1)	16·3(2)	10·9(1)	8·5(1)	1868(14)
16/6/99	52·5(2)	0·0	15·3(1)	11·4(1)	11·4(1)	9·0(1)	2126(28)
17/6/99	52·6(7)	0·0	15·4(3)	11·1(2)	11·5(2)	9·0(1)	2090(54)
10/6/99	52·5(1)	0·0	15·4(1)	11·2(1)	11·5(1)	8·9(1)	2131(51)
11/6/99	53·0(2)	0·0	15·5(1)	11·2(1)	11·6(2)	9·1(1)	2054(22)
25/6/99	55·9(1)	0·0	16·3(1)	5·5(1)	12·0(1)	9·7(1)	1576(27)
28/6/99	56·9(2)	0·0	17·5(1)	2·6(1)	13·1(1)	9·9(1)	1711(44)
30/6/99	49·3(1)	0·0	15·3(1)	15·2(1)	11·4(1)	8·6(1)	1701(28)
2/7/99	51·7(2)	0·0	15·2(1)	13·0(1)	11·4(1)	8·9(1)	2046(29)
7/7/99	53·6(1)	0·0	15·7(1)	9·2(1)	11·7(1)	9·2(1)	1785(38)
9/7/99	55·9(5)	0·0	17·4(3)	3·7(1)	12·8(2)	9·9(1)	1528(29)
Cape Vogel high-Mg andesite							
18/6/99							
13/8/99	59·0(2)	0·0	11·6(1)	9·9(1)	12·7(1)	6·4(1)	100(14)
21/6/99	59·3(3)	0·0	11·0(1)	10·0(1)	12·3(1)	6·2(1)	278(15)
22/6/99	60·0(2)	0·0	11·1(1)	10·1(1)	12·3(1)	6·3(1)	640(44)
16/6/99	60·0(2)	0·0	11·2(1)	10·1(1)	12·4(2)	6·3(1)	1480(88)
17/6/99	60·4(1)	0·0	11·2(1)	10·2(1)	12·4(1)	6·3(1)	1220(58)
10/6/99	59·7(3)	0·0	11·1(1)	9·9(1)	12·2(1)	6·2(1)	1477(37)
11/6/99	60·4(1)	0·0	11·2(1)	9·7(1)	12·4(1)	6·3(1)	1417(28)
25/6/99	62·9(3)	0·0	11·6(1)	5·7(1)	12·7(1)	6·6(1)	1374(34)
28/6/99	64·0(2)	0·0	12·6(2)	2·7(1)	13·8(1)	6·8(1)	1433(37)
30/6/99	58·9(1)	0·0	11·5(1)	9·7(1)	12·8(1)	6·3(1)	582(12)
2/7/99	60·3(2)	0·0	11·2(1)	9·9(1)	12·3(1)	6·2(1)	1042(21)
7/7/99	60·4(3)	0·0	11·2(1)	9·6(1)	12·4(1)	6·3(1)	1552(29)
9/7/99	63·0(2)	0·0	12·4(1)	3·9(1)	13·5(1)	6·7(1)	1306(15)
High-Ti mare basalt							
18/6/99							
13/8/99	38·2(6)	13·3(1)	8·3(1)	18·9(4)	10·3(2)	10·6(2)	668(15)
21/6/99	38·4(2)	13·1(1)	7·9(1)	19·1(2)	9·9(1)	10·4(1)	1935(27)
22/6/99	37·8(1)	13·0(1)	8·3(1)	18·8(2)	10·3(1)	10·5(2)	4123(32)
16/6/99	41·5(1)	14·2(1)	8·5(1)	13·5(1)	10·7(1)	11·2(1)	4900(33)
17/6/99	41·7(2)	14·1(1)	8·5(1)	13·4(1)	10·8(1)	11·2(1)	4960(158)
10/6/99	41·6(1)	14·1(2)	8·5(1)	13·5(1)	10·7(1)	11·2(1)	5027(68)
11/6/99	41·8(1)	14·2(1)	8·4(1)	13·2(2)	10·7(1)	11·3(1)	4787(67)
25/6/99	44·5(2)	15·1(2)	9·1(1)	6·8(1)	11·3(1)	12·0(1)	3999(37)
28/6/99	45·5(4)	15·3(1)	9·9(2)	3·5(1)	12·4(1)	12·4(1)	4637(65)
30/6/99	38·3(2)	13·0(1)	8·5(1)	18·3(1)	10·6(1)	10·6(1)	3958(50)
2/7/99	40·9(3)	13·8(1)	8·3(2)	14·5(1)	10·6(1)	11·0(1)	4665(48)
7/7/99	42·6(5)	14·5(2)	8·8(2)	10·8(3)	11·0(2)	11·5(1)	4226(36)
9/7/99	44·7(3)	15·3(1)	9·8(1)	4·7(1)	12·3(1)	12·4(1)	4012(35)

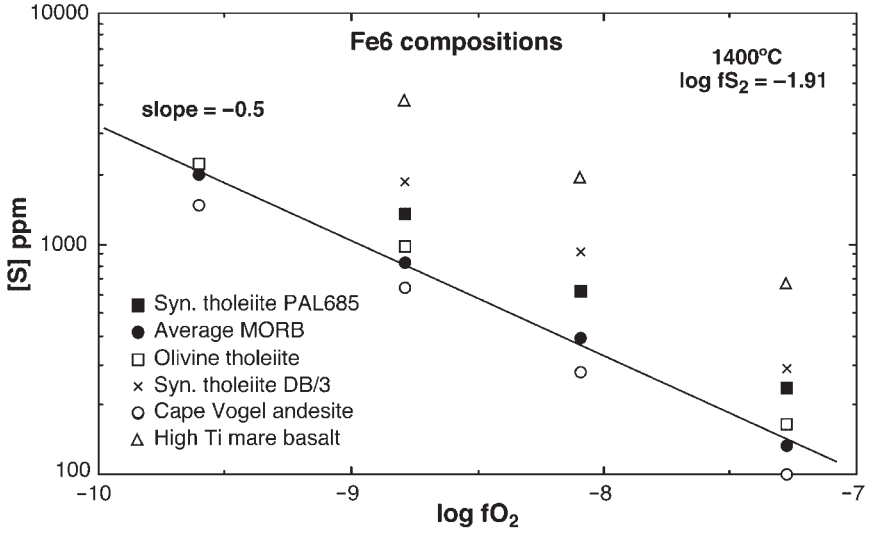

Fig. 5. S solubilities in FeS-undersaturated 'Fe6' compositions as a function of fO_2, at constant fS_2 ($\log fS_2 = -1{\cdot}91$). The theoretical slope of $-0{\cdot}5$ is shown.

Table 5: Compositions of simplified, synthetic FeO-bearing melts ('Fe6' compositions) recalculated to a FeO-free basis from data in Table 4

Composition name	Reference	SiO_2	TiO_2	Al_2O_3	MgO	CaO
Average MORB	Niu & Batiza (1993)	58·6(5)	1·5(1)	17·2(3)	8·7(2)	13·9(1)
Olivine tholeiite	McDonough *et al.* (1985)	61·0(5)	2·6(1)	16·0(3)	9·9(2)	10·6(1)
Synthetic tholeiite PAL 685	Buchanan & Nolan (1979)	69·9(5)	0·0	15·0(3)	4·6(2)	10·5(1)
Synthetic tholeiite DB/3	Buchanan & Nolan (1979)	59·1(5)	0·0	17·6(3)	13·1(2)	10·2(1)
Cape Vogel andesite	Jenner (1981)	66·5(5)	0·0	12·6(3)	13·9(2)	7·0(1)
High-Ti mare basalt	Danckwerth *et al.* (1979)	47·9(5)	16·3(1)	10·1(3)	12·6(3)	13·0(1)

A spin-off from using the AD-eutectic composition as the basis of studying compositional effects is that we have generated a number of replicate experiments on this composition at identical conditions, providing a test of the reliability of our experimental procedure. This is shown in Fig. 12.

The join AD eutectic–FeO

The FeO–'Matrix' binaries discussed so far were generated by removing FeO from the starting compositions by exsolution of FeS liquid. Thus all samples are FeS saturated with the exception of those with the original FeO content of the starting composition (allowing for minor FeO loss to the Re loops). An alternative way to study the effect of FeO on C_S is to add FeO to an original FeO-free starting composition. We have done this by adding FeO to the AD-eutectic composition. Two experiments were performed (Table 11). The earlier experiment used Pt loops and resulted in massive loss of Fe to the Pt (which illustrates well how important the use of the Re wires has been to our experimental campaign). Nevertheless, the results of this experiment are consistent with those on the Re loops (Fig. 13). More importantly, the results plot on the same slope of ln C_S vs FeO as the five 'terrestrial' Fe6 compositions, demonstrating that values of C_S are not affected by FeS saturation. Fitting the data to the same empirical relation [equation (5)] shows this. The results of the fitting are given in Table 6.

Because the value of C_S° for AD eutectic is very similar to that for the anomalous sixth composition (the high-Ti mare basalt), these data also imply that the different slope of C_S vs FeO for the high-Ti mare basalt composition is not due to its high value for C_S°.

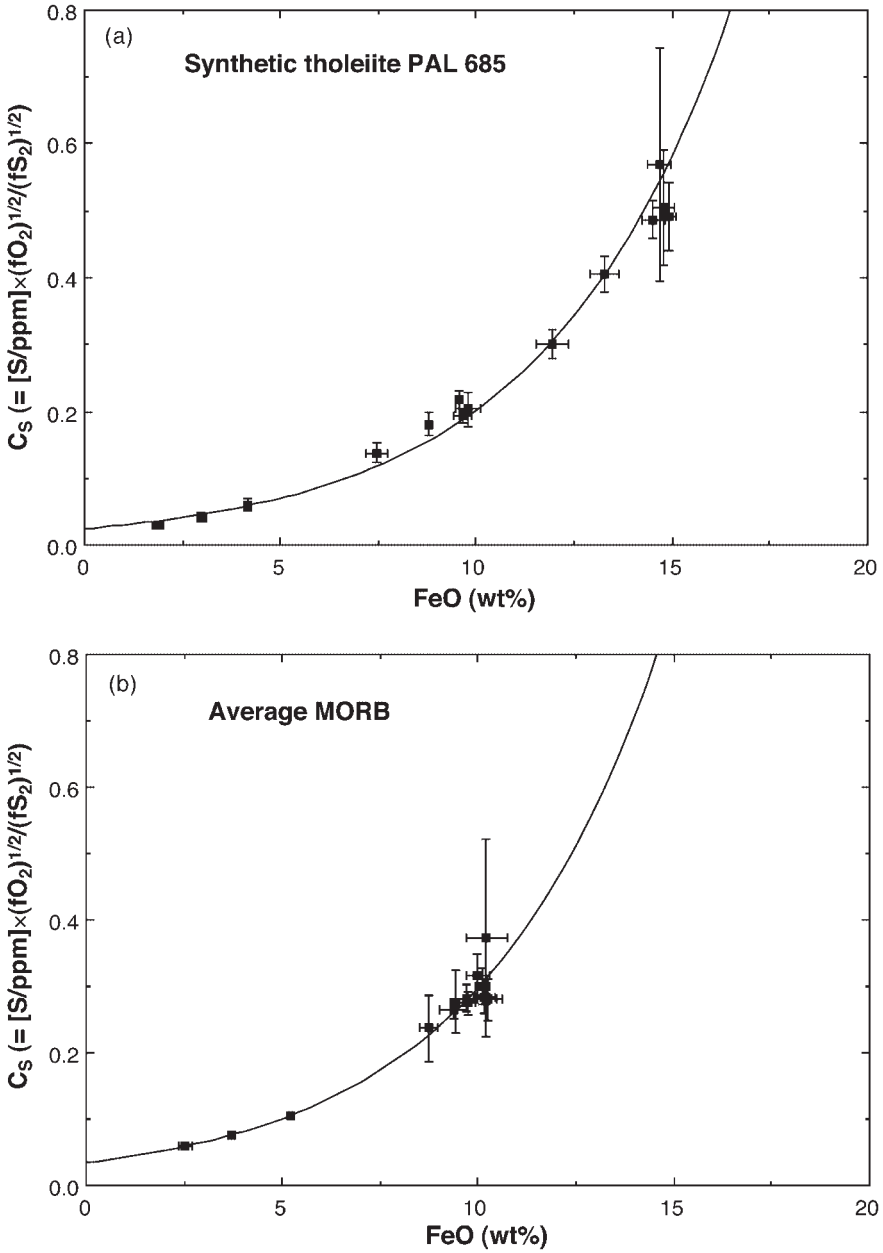

Fig. 6. Sulfide capacity, C_S, vs FeO in wt % for two 'Fe6' compositions. The curves are exponential fits to the data. These plots emphasize the great influence of the FeO content of the melt on its C_S. For basaltic compositions (with rare exceptions that have FeO >8 wt %) other aspects of their composition have only a slight effect on C_S.

THERMODYNAMIC THEORY

Thermodynamic theory of the compositional dependence of the sulfide capacity, C_S

The choice of the thermodynamic components used to describe the thermodynamic properties of silicate melts is to some extent discretionary. If the simplest-looking components, namely the single oxide components (SiO_2, MgO, FeO, etc.), are used, deviations from ideal thermodynamic mixing can be fairly complex, requiring the use of impractically complex mixing models. Conversely, it has long been appreciated that more complex components that mimic the stoichiometry of common silicate minerals mix almost ideally, and this approach currently underlies most practical thermodynamic modelling of silicate liquids in the geological literature. However, it is not immediately obvious how the modelling of sulfide

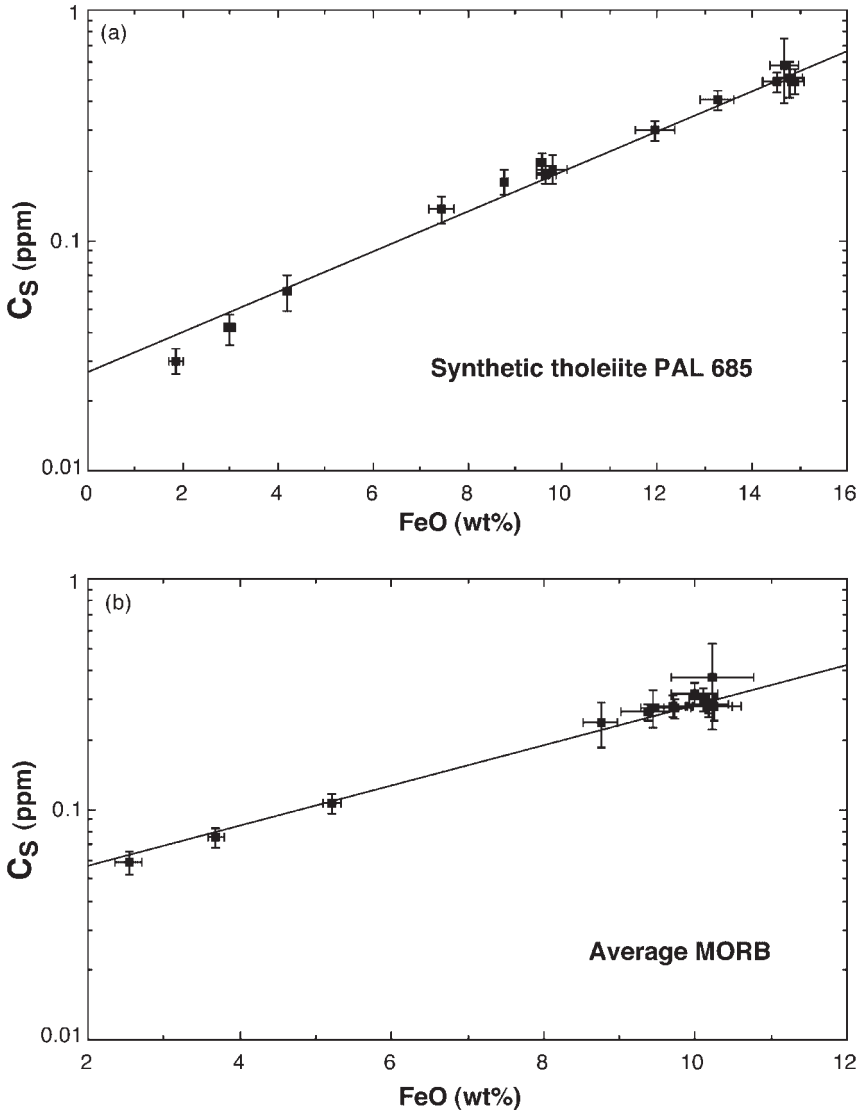

Fig. 7.

capacities can best be grafted onto this approach. As the purpose of this section is to derive an appropriate algebraic form for the dependence of C_S on composition, we shall begin using the simple oxide components. We briefly discuss the implications of using a mineral-stoichiometry approach in a later section.

As the Fincham–Richardson theory envisages S^{2-} replacing O^{2-} on the anion sublattice, it is convenient to define the oxide components of the silicate melt in terms of a single oxygen ion (e.g. $Si_{0.5}O$, $Ti_{0.5}O$, $Al_{0.67}O$, CaO, Na_2O, etc.) and the sulfide components as $Si_{0.5}S$, $Ti_{0.5}S$, $Al_{0.67}S$, CaO, Na_2S, etc.

The concept of mixing on different sublattices logically requires that the activities of the M_zO and M_zS components be formulated in the context of the reciprocal solution model, which was first developed for molten salts (Flood *et al.*, 1954), and introduced into the geological literature (for crystalline solid solutions) by Wood & Nicholls (1978). In this formulation, the total free energy of the solution comes from three kinds of contributions:

(1) the sum of the free energies of the pure end-member components, weighted according to the mole fractions of these components:

$$G^{\circ}_{\text{end-members}} = \sum_{M,X} X^{\text{cat}}_{M} X^{\text{an}}_{X} \mu^{\circ}_{MzX} \qquad (6)$$

(2) ideal mixing of cations and anions on each sublattice:

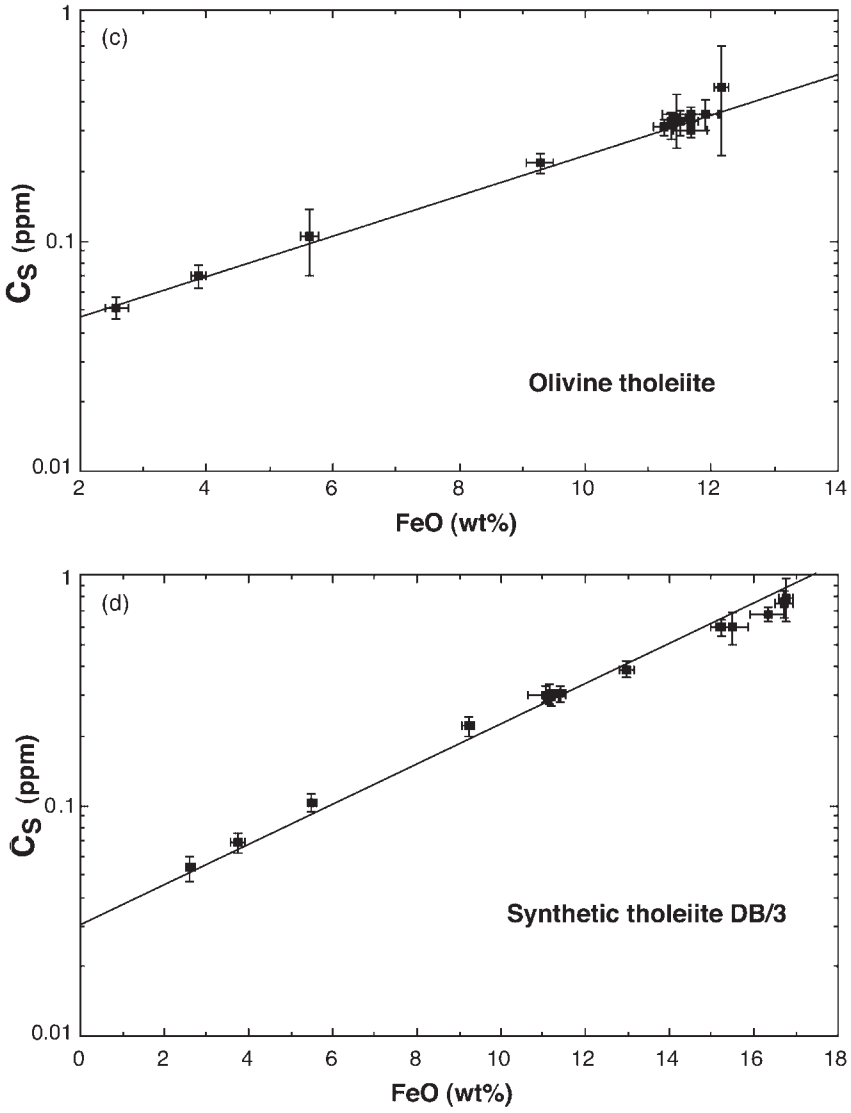

Fig. 7.

$$G^{\circ}_{\text{ideal mixing}} = -RT\left[\sum_{\mathrm{M}} zX^{\text{cat}}_{\mathrm{M}} \ln\left(X^{\text{cat}}_{\mathrm{M}}\right) + \sum_{\mathrm{M}} zX^{\text{an}}_{X} \ln(X^{\text{an}}_{X})\right] \tag{7}$$

(3) excess free energies of mixing, which account for deviations from the ideal mixing on sublattices given by the $G^{\circ}_{\text{ideal mixing}}$ term. This contribution is expressed empirically using activity coefficients for cations and anions separately on each sublattice:

$$G^{\circ}_{\text{excess}} = -RT\left[\sum_{\mathrm{M}} zX^{\text{cations}}_{\mathrm{M}} \ln(\gamma^{\text{cat}}_{\mathrm{M}}) + \sum_{\mathrm{M}} X^{\text{anions}}_{X} \ln(\gamma^{\text{an}}_{X})\right] \tag{8}$$

where $\gamma^{\text{cat}}_{\mathrm{M}}$ and γ^{an}_{X} are functions of the other cations and anions (respectively) on each sublattice, but it is assumed that there are no interactions between the sublattices, i.e. $\gamma^{\text{cat}}_{\mathrm{M}}$ does not depend on the composition of the anion sublattice nor γ^{an}_{X} on the cation sublattice. Unfortunately, as far as we know, this important assumption has never been tested against experimental measurement for any silicate system, liquid or solid.

The mole fractions of both the cations on the cation sublattice and the anions on the anion sublattice are taken to sum to unity, i.e. we assume no vacant sites.

For any oxide component $\mathrm{M}_z\mathrm{O}$, there is a reaction

$$\mathrm{M}_z\mathrm{O} + \tfrac{1}{2}\mathrm{S}_2 = \mathrm{M}_z\mathrm{S} + \tfrac{1}{2}\mathrm{O}_2. \tag{9}$$

(It should be noted that the Fincham–Richardson theory

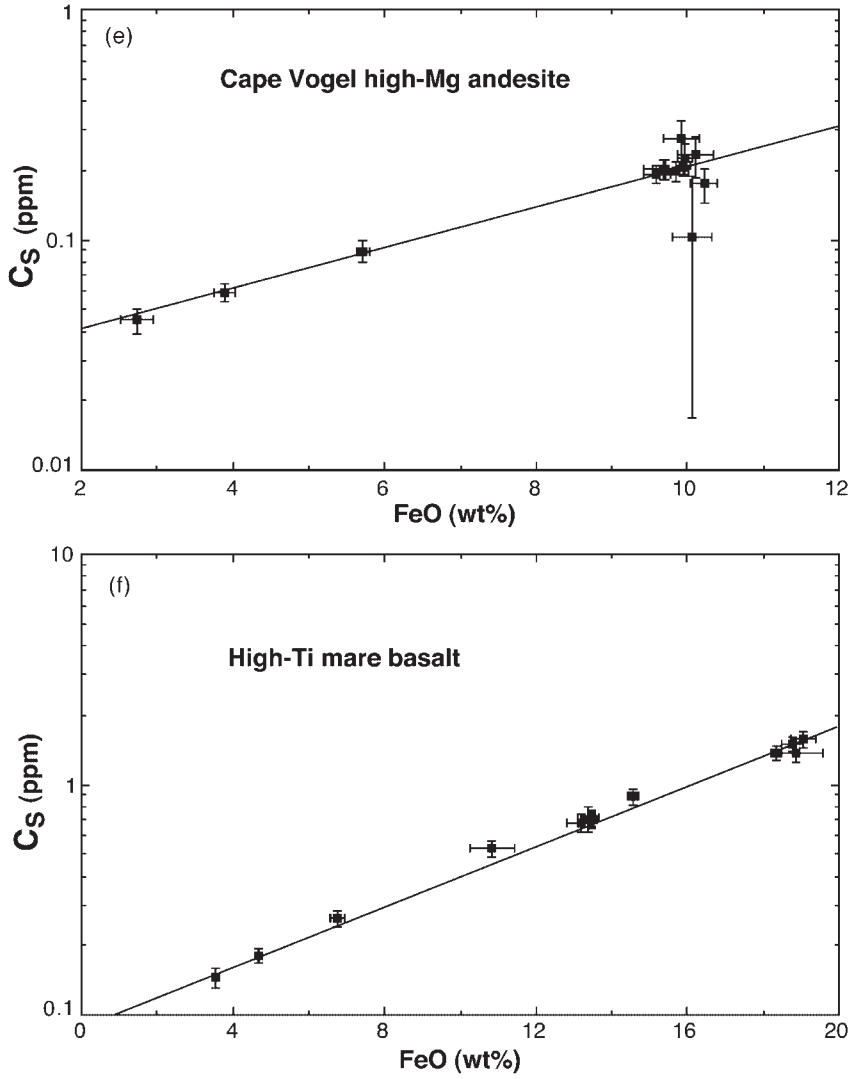

Fig. 7. C_S (logarithmic scale) vs FeO for all six 'Fe6' compositions.

implies that z must be the same in M_zO and M_zS for each M.) Hence at equilibrium

$$\mu_{M_zS} + \tfrac{1}{2}\mu_{O_2} - \mu_{M_zO} + \tfrac{1}{2}\mu_{S_2} = 0 \qquad (10)$$

where

$$\mu_{O_2} = RT \ln fO_2 \qquad (11)$$

$$\mu_{S_2} = RT \ln fS_2 \qquad (12)$$

$$\mu_{M_zO} = \mu^\circ_{M_zO} + \sum_{N(\neq M)} (X_N X_S . \Delta\mu^\circ_{rec}) + zRT \ln (X_M) + RT \ln (X_O) + RT \ln (\gamma_M) + RT \ln (\gamma_O) \qquad (13)$$

$$\mu_{M_zS} = \mu^\circ_{M_zS} + \sum_{N(\neq M)} (- X_N X_O . \Delta\mu^\circ_{rec}) + zRT \ln (X_M) + RT \ln (X_S) + RT \ln (\gamma_M) + RT \ln (\gamma_S) \qquad (14)$$

and

$$\Delta\mu^\circ_{rec} = \mu^\circ_{M_zS} + \mu^\circ_{N_zO} - \mu^\circ_{M_zO} + \mu^\circ_{N_zS}. \qquad (15)$$

It should be noted that $X_S + X_O = 1$ and $X_M = 1 - \Sigma X_N$. From the assumption that deviations from ideal mixing on the cation and anion sublattices are independent of each other, for small amounts of S^{2-} dissolved in the melt, $X_O \approx 1$, hence $\gamma_O = 1$ by definition, and γ_S is a constant (i.e. Henry's law). This is effectively the same approximation as used by Fincham & Richardson

Table 6: Results of fitting the sulfide capacities (C_S) of Fe-bearing compositions to the relation $C_S = C_S^\circ\ (1 - c_{FeO}]/100)\ exp\{B.c_{FeO}/100\}$, where c_{FeO} is the amount of FeO in wt % and C_S° is the sulfide capacity of the Fe-free composition renormalized to 100% (given in Table 3)

Composition	C_S° (ppm)	B	χ^2_ν	Number of data
Average MORB	0·038(1)	20·9(2)	1·49	68 (Table 4)
Olivine tholeiite	0·032(1)	20·9(2)		
Synthetic tholeiite PAL 685	0·026(8)	20·9(2)		
Synthetic tholeiite DB/3	0·030(1)	20·9(2)		
Cape Vogel andesite	0·028(1)	20·9(2)		
High-Ti mare basalt	0·092(5)	16·1(4)	0·68	13 (Table 4)
AD eutectic + FeO	0·090(4)	19·5(7)	0·74	11 (Table 11)

The first five compositions were treated together, assuming a constant value of B. It should be noted that the data include compositions both saturated and undersaturated in immiscible FeS melt.

Table 7: Effect of adding SiO_2 and Al_2O_3 to the An–Di eutectic composition in the system CMAS

SiO_2	Al_2O_3	MgO	CaO	S (ppm)
AD + SiO_2, log $fO_2 = -10{\cdot}92$, log $fS_2 = -1{\cdot}91$, 40 h (10/7/99)				
50·4(1)	14·9(1)	10·4(1)	23·9(2)	2720(29)
55·5(4)	13·5(1)	9·3(1)	21·6(1)	1944(31)
59·8(2)	12·1(1)	8·5(1)	19·3(1)	1606(14)
65·2(3)	10·6(2)	7·4(1)	16·9(1)	1234(23)
65·8(4)	10·2(1)	7·1(1)	16·3(1)	1145(23)
AD + SiO_2, log $fO_2 = -10{\cdot}92$, log $fS_2 = -1{\cdot}91$, 44 h (16/8/99)				
50·7(2)	15·1(1)	10·4(1)	23·9(1)	2711(39)
53·5(4)	14·2(1)	9·8(1)	22·4(2)	2270(43)
56·6(1)	13·1(1)	9·1(1)	20·9(1)	1944(66)
60·4(2)	12·1(1)	8·3(1)	19·2(1)	1537(50)
AD + Al_2O_3, log $fO_2 = -9{\cdot}60$, log $fS_2 = -1{\cdot}91$, 20 h (29/3/97)				
50·7(3)	14·8(1)	10·1(1)	24·2(2)	584(22)
48·1(2)	19·1(1)	9·4(1)	23·2(1)	568(10)
45·3(2)	23·5(1)	9·0(1)	22·2(1)	549(18)
42·7(2)	27·2(10)	8·7(12)	20·8(2)	443(74)
42·6(1)	29·0(32)	6·5(34)	20·9(2)	390(90)
50·1(2)	14·4(1)	9·7(1)	24·3(3)	660(24)*

*Also contains 1·1(1) Cr_2O_3.

(1954) in defining C_S. Substituting (11)–(14) into (10) and rearranging gives

$$\ln X_S = -\ln \gamma_S + \sum_M X_M(\mu^\circ_{M_2O} - \mu^\circ_{M_2S})/RT + \tfrac{1}{2}\ln(fS_2/fO_2). \quad (16)$$

The definition of the sulfide capacity, C_S is

$$\ln C_S = \ln[S] + \tfrac{1}{2}\ln(fO_2/fS_2). \quad (2)$$

Combining equations (2) with (16) eliminates the term in $(fO_2/fS_2)^{1/2}$, and shows that the equation relating C_S to silicate melt composition requires the form

Table 8: Some binary joins in the system CMAS; all at log $fO_2 = -9{\cdot}60$, *log* $fS_2 = -1{\cdot}91$

SiO_2	Al_2O_3	MgO	CaO	S (ppm)
Diopside–anorthite, 16·2 h (15/3/99)				
56·4(2)	0·0	17·3(1)	26·8(1)	777(109)
52·2(2)	8·7(1)	14·2(1)	25·4(1)	756(24)
52·5(1)	10·7(1)	12·2(1)	25·5(1)	691(18)
50·3(2)	16·1(1)	9·6(1)	24·6(1)	605(22)
49·0(4)	21·9(2)	7·0(1)	23·8(2)	498(29)
A CMAS composition plus Mg_2SiO_4 *or* $MgSiO_3$, *23 h (12/12/96)*				
50·5(5)	16·1(2)	8·7(2)	24·3(2)	585(16)
50·3(3)	15·2(1)	11·4(1)	23·0(1)	605(25)
50·0(5)	14·6(4)	13·9(4)	22·0(6)	636(23)
51·8(1)	15·2(1)	9·8(1)	22·8(1)	436(15)
54·1(2)	11·8(2)	15·8(1)	18·0(1)	543(23)
55·1(2)	10·2(1)	18·8(1)	15·4(1)	480(34)
A CMAS composition plus $CaSiO_3$, *9 h (23/12/96)*				
50·5(2)	15·1(1)	6·1(1)	27·9(2)	661(38)
50·4(1)	13·3(1)	5·3(1)	30·4(1)	760(17)
50·3(1)	11·7(1)	4·7(1)	32·4(2)	825(32)
50·8(1)	10·1(1)	4·0(1)	35·4(1)	955(22)
50·9(2)	8·3(1)	3·2(1)	37·9(1)	1119(30)
50·9(2)	7·3(1)	2·8(1)	39·7(1)	1237(25)

$$\ln C_S = A_0 + \sum_M X_M A_M \quad (17)$$

where

$$A_0 = -\ln k_S \gamma_S + \text{constant} \quad (18)$$

$$A_M = (\mu^\circ_{M_zO} - \mu^\circ_{M_zS})/RT - \text{constant}. \quad (19)$$

The term k_S is to convert from mole fractions of sulfide (X_S) to parts per million (ppm); although it is not strictly a constant, it varies little over the entire range of silicate melts considered in this study, and will therefore be ignored for the convenience of working with S concentrations in ppm. The 'constant' term in (18) and (19) appears because the A_0 and A_M terms cannot be uniquely determined from (17), because ΣX_M is constrained to be unity.

The form of this equation is that adopted previously by Haughton *et al.* (1974). The importance of the thermodynamic derivation presented here is that it shows that the coefficients A_M should be directly related to the difference in the free energies of formation of the components, i.e. $(\mu^\circ_{M_zS} - \mu^\circ_{M_zO})/RT$. This is something that can be readily tested using our experimental results.

DATA FITTING AND TESTING THE MODEL

Data fitting by non-linear least-squares regression

To fit the data, we adopted the expression

$$\ln C_S = A_0 + A_{Ca}X_{Ca} + A_{Mg}X_{Mg} + A_{Al}X_{Al} + A_{Na/K}(X_{Na} + X_K) + A_{Ti}X_{Ti} + A_{Fe}X_{Fe} \pm B_{Fe-Ti}X_{Fe}X_{Ti}. \quad (20)$$

The last term is an empirical addition to the equation as derived theoretically, and was included to account for the anomalous slope of C_S vs FeO found for the high-Ti lunar mare basalt composition (see Table 6). The data were fitted both with and without this term.

The silicate melt compositions in wt % given in the tables were converted to mole fractions on the cation sublattice according to

$$X_{Si} = \frac{c_{SiO_2}/60{\cdot}09}{(c_{SiO_2}/60{\cdot}09) + (2c_{Al_2O_3}/101{\cdot}96) + (c_{CaO}/56{\cdot}08) + (2c_{Na_2O}/61{\cdot}98) + \ldots} \quad (21)$$

and so on for the other oxides. We set $A_{Si} = 0$, as the constraint that $\sum_M X_M = 1$ means that the equation would

Table 9: Effect of TiO_2

SiO_2	TiO_2	Al_2O_3	FeO	MgO	CaO	S (ppm)
AD eutectic + TiO_2, log $fO_2 = -9{\cdot}60$, log $fS_2 = -1{\cdot}91$ (6/2/97)						
47·7(2)	5·1(1)	14·1(1)	0	9·5(1)	23·2(2)	721(21)
44·8(2)	9·7(1)	13·4(1)	0	9·2(1)	21·9(1)	799(8)
42·5(1)	14·9(1)	12·5(1)	0	8·5(1)	20·8(1)	832(24)
40·0(2)	19·7(1)	11·8(1)	0	8·0(1)	19·7(1)	894(19)
Av. MORB + TiO_2, log $fO_2 = -8{\cdot}79$, log $fS_2 = -1{\cdot}91$ (18/8/99)						
52·6(2)	1·4(1)	15·2(1)	10·1(1)	7·7(1)	12·4(1)	827(27)
52·4(3)	1·3(1)	15·9(1)	9·7(1)	8·2(1)	12·6(1)	728(23)
48·8(2)	7·3(1)	14·8(1)	9·1(2)	7·5(1)	11·8(1)	733(20)
47·6(2)	9·8(1)	14·6(1)	9·0(1)	7·5(1)	11·6(1)	734(18)
46·0(1)	12·9(1)	13·9(2)	8·7(1)	7·0(1)	11·1(1)	726(15)
44·5(1)	15·8(2)	13·6(1)	8·4(2)	6·9(1)	10·8(1)	708(21)
43·4(2)	17·7(2)	13·2(1)	8·1(1)	6·8(1)	10·5(1)	735(45)
Cape Vogel High-Mg andesite + TiO_2, log $fO_2 = -8{\cdot}79$, log $fS_2 = -1{\cdot}91$ (24/8/99)						
60·0(2)	0·0	11·1(1)	10·1(1)	12·3(1)	6·3(1)	640(44)
55·5(2)	6·1(1)	10·7(1)	9·1(1)	11·9(2)	6·0(1)	532(24)
51·6(3)	12·3(1)	10·1(1)	8·4(1)	11·2(1)	5·5(1)	476(19)
50·5(3)	13·9(1)	9·7(1)	8·3(1)	10·8(1)	5·4(1)	541(24)
48·7(2)	16·8(1)	9·5(1)	8·1(1)	10·6(1)	5·3(1)	538(16)

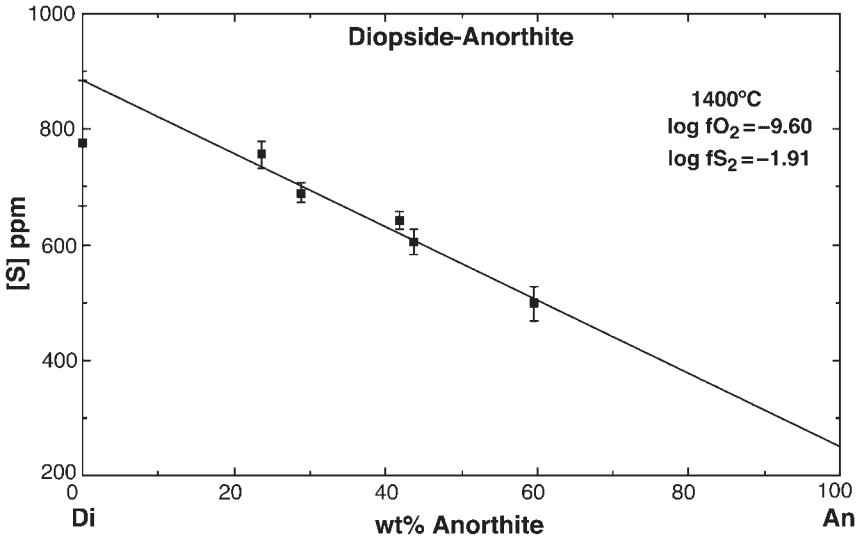

Fig. 8. S solubility at $\log fO_2 = -9{\cdot}60$, $\log fS_2 = -1{\cdot}91$ across the $CaMgSi_2O_6$–$CaAl_2Si_2O8$ binary join (anorthite–diopside).

be over-determined if all the oxide components were used. Haughton *et al.* (1974) also set $A_{Al} = 0$, and we decided to test this option too.

We included the following experimental data, weighted for non-linear least-squares regression using the uncertainties in analysed compositions propagated through equation (20), and uncertainties in C_S calculated from the uncertainties in [S], fO_2 and fS_2 as indicated:

(1) 12 CMAS compositions plus one CMAS–TiO_2 composition, from Table 1, using values of C_S and the

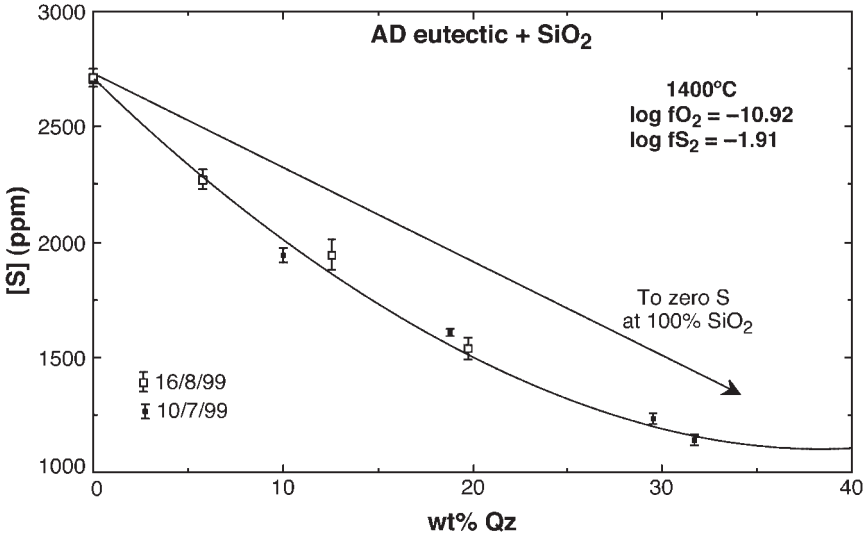

Fig. 9. Effect of adding SiO_2 to anorthite–diopside eutectic composition (ADeu). The trend is fitted well by an exponential curve.

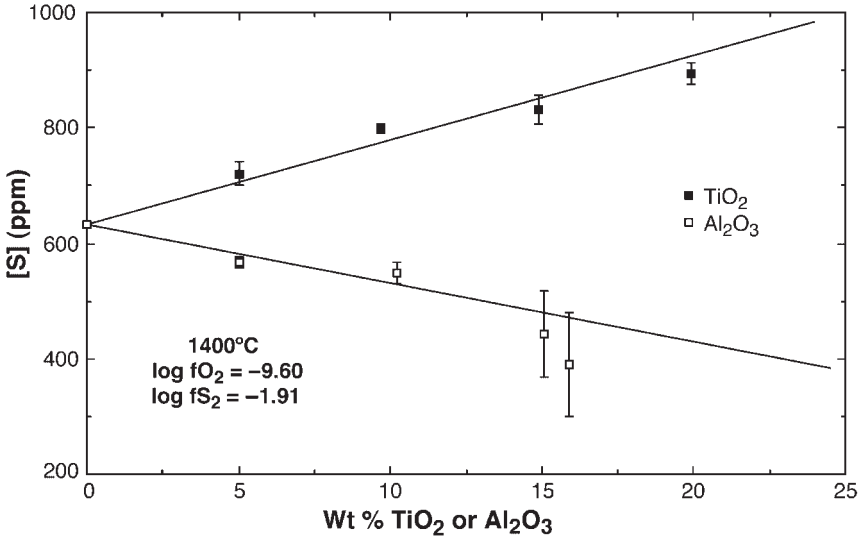

Fig. 10. Effect of adding Al_2O_3 and TiO_2 to the ADeu composition.

standard deviations of these values, also given in Table 1; these data were obtained from 133 experiments (Table 2);

(2) 31 more CMAS data (Tables 7 and 8), nine CMAS–Na_2O and five CMAS–K_2O data (Table 10) and four CMAS–TiO_2 data (Table 9), weighted assuming $\pm 0{\cdot}05$ in $\log fO_2$ and $\log fS_2$, and either the observed standard deviation of the EMP analyses as given in the tables, or 5% of [S], whichever is the larger;

(3) 81 CMAS–TiO_2–FeO compositions from Table 4, and 11 compositions from ADeu–FeO (Table 11), weighted as above, but assuming $\pm 0{\cdot}03$ in $\log fO_2$ and $\log fS_2$.

Thus 274 experiments were used. The result of the regressions, both with and without the terms in A_{Al} and B_{Fe-Ti}, are summarized in Table 12.

The value of the reduced chi-squared (χ^2_ν) for the regression including both the A_{Al} and B_{Fe-Ti} terms is 2·33, which is higher than that required for a satisfactory fit, given the assumed uncertainties in the input data (the value of χ^2_ν should be unity for a large number of data if the uncertainties in the input data are estimated correctly). The A_{Al} parameter is only of marginal significance and setting this parameter to zero increases the value of χ^2_ν only to 2·57. However, the B_{Fe-Ti} term is significant and leaving out this term increases χ^2_ν to 4·00.

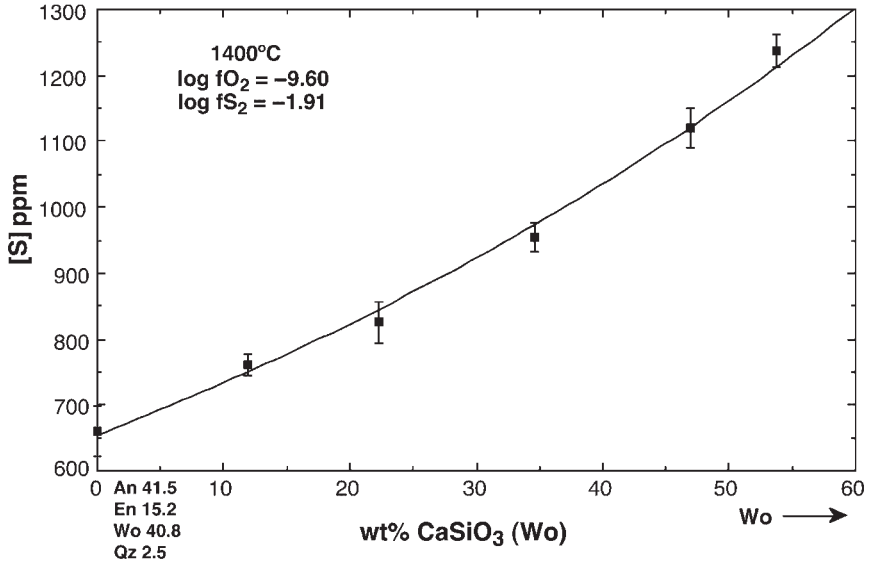

Fig. 11. Effect of adding $CaSiO_3$ to a CMAS composition near the ADeu composition. The trend is well fitted by an exponential curve.

Table 10: Effect of alkalis (Na and K); all at log $fO_2 = -9{\cdot}60$, *log* $fS_2 = -1{\cdot}91$

SiO_2	Al_2O_3	MgO	CaO	Na_2O	S (ppm)
AD eutectic + albite (22/3/97)					
50·7(1)	14·8(1)	10·1(1)	24·6(2)	0·2(2)	655(19)
59·5(2)	17·3(1)	6·2(1)	15·4(1)	1·7(1)	219(16)
64·4(2)	18·2(1)	4·1(1)	10·3(1)	3·0(2)	151(29)
68·8(6)	19·4(2)	1·7(1)	4·7(2)	3·9(4)	42(14)
72·3(2)	20·6(2)	0·0	0·1(1)	5·2(3)	23(18)
AD eutectic + Na-metasilicate (1/4/97)					
50·5(2)	14·8(1)	10·1(1)	24·5(1)	0·6(1)	683(24)
68·7(1)	9·3(1)	5·3(1)	13·7(1)	2·8(1)	259(19)
74·5(6)	7·2(1)	4·1(2)	11·2(5)	2·8(1)	240(44)
86·1(2)	0·5(1)	0·1(1)	0·9(1)	11·0(1)	139(20)
SiO_2	Al_2O_3	MgO	CaO	K_2O	S (ppm)
AD eutectic + orthoclase (30/3/97)					
50·8(1)	14·8(1)	10·1(1)	24·2(1)	0·1(1)	656(30)
53·4(2)	15·3(1)	9·1(1)	22·4(1)	0·3(1)	498(21)
55·0(1)	16·1(1)	8·2(1)	20·4(1)	0·4(1)	419(26)
57·3(2)	16·7(1)	7·3(1)	18·1(1)	0·9(1)	345(26)
59·2(2)	17·2(1)	6·2(1)	15·5(1)	1·4(1)	293(28)

The uncertainties in each parameter from the regressions are also presented to indicate the effectiveness with which the parameter is constrained by the range of compositions studied. Because there is a fairly high correlation between some of these parameters, full error propagation would require the complete error matrix including cross-terms. Obviously, for a seven- or eight-parameter model this involves a tedious number of terms (28 or 36, respectively), and it suffices to note that the input values of C_S are reproduced with a root-mean

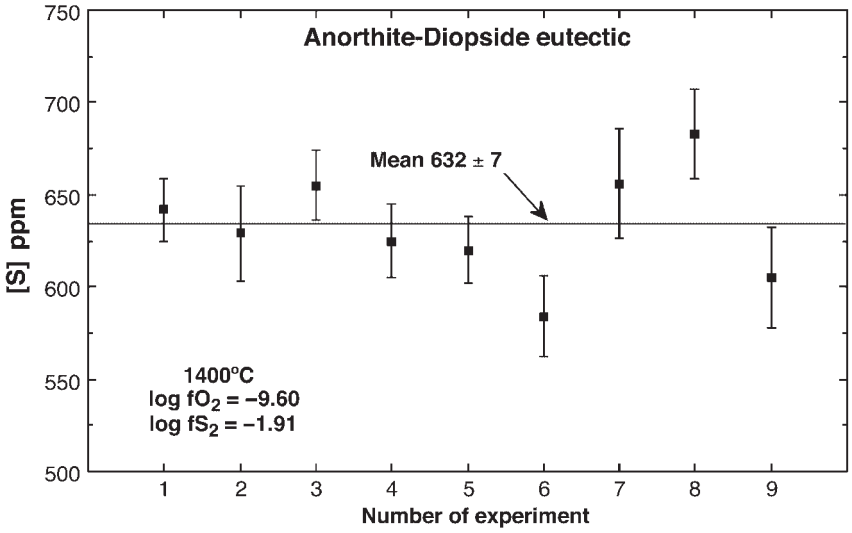

Fig. 12. Replicate measurements on the ADeu composition at $\log fO_2 = -9{\cdot}60$ and $\log fS_2 = -1{\cdot}91$. These experiments were run over a period of more than 2 years and analysed in different sessions over a similar period. The mean and standard error of the mean are given.

Table 11: AD eutectic + FeO

SiO_2	Al_2O_3	FeO	MgO	CaO	S (ppm)
On Re: log $fO_2 = -8{\cdot}79$, log $fS_2 = -1{\cdot}91$ (2/9/99)					
49·9(2)	14·9(1)	1·62(6)	10·2(1)	23·3(1)	390(23)
48·4(2)	14·5(1)	4·65(6)	10·0(1)	22·6(1)	655(52)
47·8(3)	14·4(1)	5·04(4)	10·0(1)	22·5(1)	704(23)
47·5(2)	14·0(1)	6·35(5)	9·7(1)	22·1(1)	900(26)
46·4(3)	13·9(1)	8·46(22)	9·7(1)	21·6(1)	1324(65)
46·1(1)	13·9(1)	8·74(11)	9·5(1)	21·6(1)	1301(30)
45·7(1)	13·6(1)	9·35(18)	9·5(1)	21·3(1)	1372(122)
On Pt: log $fO_2 = -9{\cdot}60$, log $fS_2 = -1{\cdot}91$ (27/3/97)					
50·2(9)	15·2(3)	0·00	10·1(1)	25·0(4)	620(18)
51·3(5)	14·7(2)	0·57(34)	9·8(2)	24·3(5)	629(22)
50·6(6)	14·8(2)	0·95(19)	10·0(1)	24·5(1)	727(14)
50·1(4)	14·6(2)	2·14(61)	9·9(1)	24·2(1)	1018(24)

square deviation (RMSD) of 9% (eliminating seven runs with very low S and consequently very high uncertainty). A detailed examination of the residuals of the regression shows that probably only the value of C_S for one composition, namely CMAS-E, is significantly misfit. The calculated value of C_S for this composition is 0·104, which is ~20% lower than the experimentally measured value of 0·125 (Table 1). But because the experimentally measured value is derived from 10 separate experiments (Table 2), we have confidence in it, and this anomaly must be taken as a real indication that the model does not provide a perfect description of C_S at all possible silicate melt compositions. The quality of the fit for the eight-parameter model is demonstrated in Fig. 14.

Further experimental tests

The data in Table 13 on the ADeu–Fe_2SiO_4–SiO_2 system and in Table 14 on the ADeu composition with variable FeO substituting for MgO were not included in the regression as most experiments were on Pt loops and accordingly suffered heavy Fe loss. On these grounds their reliability might be considered dubious. On the other

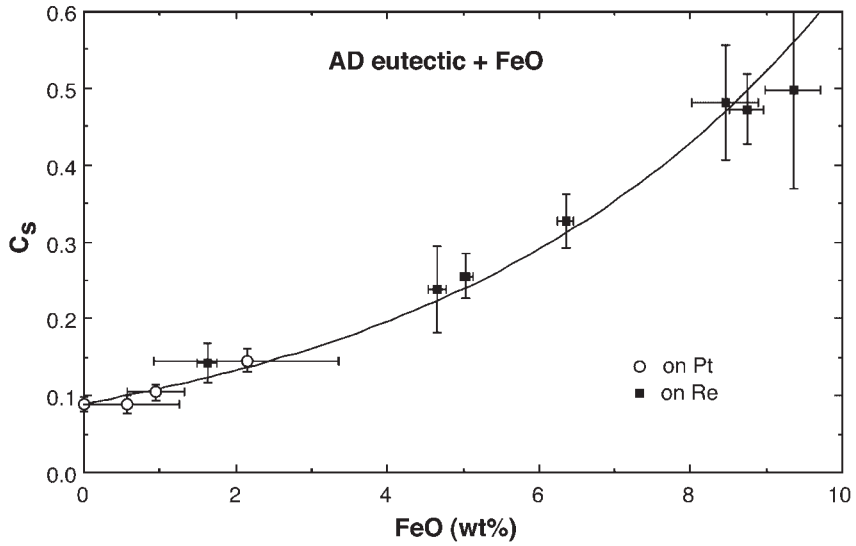

Fig. 13. C_S vs wt % FeO for ADeu plus FeO. All samples are undersaturated in FeS. The experiments on Pt wire have lost most of their original FeO, but still plot on the same curve as those on Re.

Table 12: Results of data fitting by non-linear least-squares to the expression ln $C_S = A_0 + A_{Ca}X_{Ca} + A_{Mg}X_{Mg} + A_{Fe}X_{Fe} + A_{Na/K}(X_{Na} + X_K) + A_{Ti}X_{Ti} \pm A_{Al}X_{Al} \pm B_{Fe-Ti}X_{Fe}X_{Ti}$, *where* $C_S =$ *[S (in ppm)]* $(fO_2/fS_2)^{1/2}$

Parameter	8 terms		7 terms		7 terms	
	value	SD	value	SD	value	SD
A_0	−5·018	0·050	−4·834	0·055	−4·779	0·040
A_{Ca}	7·56	0·13	7·00	0·12	7·28	0·12
A_{Mg}	4·48	0·13	3·87	0·12	4·24	0·12
$A_{Na/K}$	4·24	0·79	2·70	0·78	3·25	0·77
A_{Ti}	5·20	0·21	3·21	0·16	5·13	0·21
A_{Fe}	26·31	0·24	24·17	0·19	26·15	0·23
A_{Al}	1·06	0·18	1·48	0·17	—	—
B_{Fe-Ti}	48·48	3·10	—	—	−51·27	3·06
χ^2_ν	2·33		4·00		2·57	

hand, there is demonstrably good agreement between Pt-loop and Re-loop experiments on the related join ADeu–FeO (Fig. 13). Accordingly, we decided that the best use of these data was as a test of the other results. The comparison between observed and calculated values of C_S is made in Fig. 15. Although most data are fitted well by the model, we draw attention to three data points at high FeO contents (>20 wt %), which lie on a trend away from the one-to-one correlation line (Fig. 15). This is an indication that the model breaks down at very high FeO contents, in the range relevant to lunar basalts and other extraterrestrial compositions. Future work will address this issue.

We also further tested the need for the B_{Fe-Ti} term to describe high FeO and TiO_2 compositions, by adding TiO_2 to two of the low-Ti 'Fe6' compositions, namely the 'average MORB' and the 'Cape Vogel high-Mg andesite'. Results are given in Table 9. For the seven-term model (i.e. without the B_{Fe-Ti} term), the RMSD between calculated and observed values of C_S is 8%, whereas for the eight-term model (with the B_{Fe-Ti} term), the RMSD is only 3·6%, thus confirming the desirability

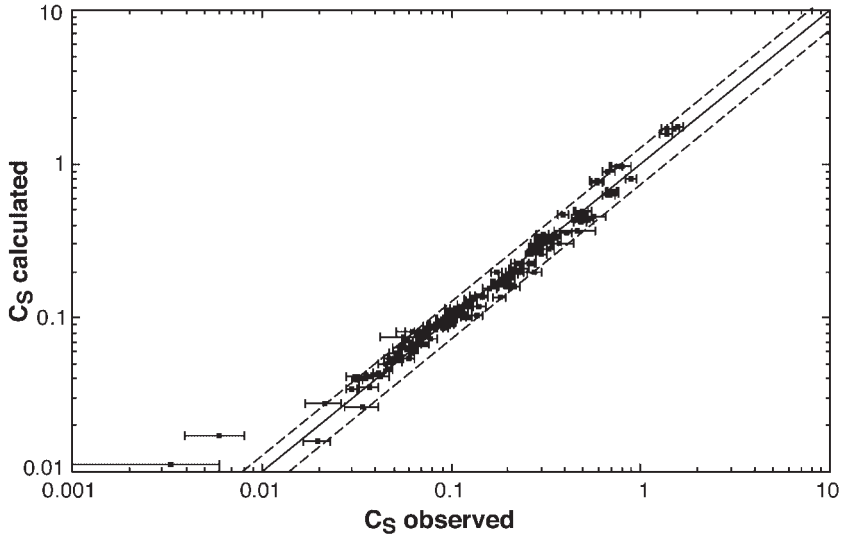

Fig. 14. Sulfide capacities observed vs calculated from equation (19), using coefficients for the seven-term model (with $A_{Al} = 0$) in Table 12. Dashed lines delineate ±25% deviations from the 1:1 line. The two rather anomalous samples at very low C_S are the $NaAlSi_3O_8$–Al_2O_3–SiO_2 composition (i.e. albite with Na loss) and a similar high Na–Al–Si composition, from Table 10.

of including this extra term. The match between calculated and observed values, using the eight-term model, is given in Fig. 16.

We also performed a few experiments based on a high-K_2O basaltic composition (Table 15), which we had previously used for investigating sulfide saturation in high-P experiments (Mavrogenes & O'Neill, 1999). The comparison between calculated and observed values of C_S for these data is shown in Fig. 17.

COMPARISON WITH PREVIOUS WORK

Danckwerth *et al.* (1979)

The high-Ti mare basalt composition was selected for this study partly because it had been used previously in an experimental study of S solubility, by Dankwerth *et al.* (1979), at lower T (mainly 1250°C with a few results at 1200 and 1300°C). Their experimental approach was similar to that used here, but with samples suspended on Fe-plated Pt wire. Their experiments were conducted over a range of both fO_2 and fS_2; at most of these conditions, variable amounts of immiscible FeS liquid exsolved causing a decrease of the FeO content of the silicate melt, just as in this study. Hence their original composition changes along a binary between an FeO-free end-member or 'Matrix' composition, and FeO, and their results may conveniently be assessed and compared with ours by plotting log C_S vs FeO (Fig. 18). Their data plot on a line with identical slope to our data, but displaced to lower values of log C_S by 0·4 units. This is in agreement with the trend for C_S to decrease with T that is well established in the metallurgical literature (e.g. Young *et al.*, 1992). Future experiments will allow more exact comparison. In the mean time, it is interesting to note that the exact parallelism of the slopes of log C_S vs FeO at 1400 and 1250°C suggests that only the A_0 term in equation (17) depends significantly on T.

Haughton *et al.* (1974)

In a study of somewhat similar scope to that reported in this paper, Haughton *et al.* (1974) investigated the solubility of S in Fe-containing silicate melts of approximately basaltic composition, as a function of melt composition and fO_2 and fS_2. They employed an experimental approach similar to that in our work, using CO–CO_2–SO_2 gas mixtures at atmospheric P, with quenched run products analysed by EMP. They reported 101 results, 100 of which were at 1200°C and one at 1300°C. The major difference in experimental technique was that the samples were held in alumina crucibles rather than on Re wire loops, and were stirred with alumina rods to decrease the equilibration time. The alumina crucibles and rods reacted with the silicate melt during the experiment to form spinel. This means that the major-element composition of the melt changes with time during the experiment. Most of their experiments were saturated in immiscible sulfide, and often also contained crystalline phases, mainly olivine and plagioclase. In principle, this should not affect matters, and a direct comparison of their results with ours is possible, provided, of course, that allowance is made for the

Table 13: AD eutectic plus Fe_2SiO_4

SiO_2	Al_2O_3	FeO	MgO	CaO	S (ppm)
On Re, log $fO_2 = -8{\cdot}79$, log $fS_2 = -1{\cdot}91$, 24·8 h (30/8/99)					
49·6(3)	14·0(1)	6·6(1)	9·9(1)	19·9(1)	949(18)
48·3(1)	13·4(1)	7·6(1)	9·3(1)	21·0(1)	983(24)
48·1(2)	13·4(1)	8·9(1)	9·4(1)	19·8(1)	1329(32)
46·9(3)	12·6(1)	11·7(1)	8·8(1)	19·6(1)	1789(26)
47·0(3)	12·5(1)	12·8(1)	8·8(2)	18·2(2)	2279(102)
45·7(1)	11·9(1)	15·0(1)	8·4(1)	17·9(1)	3004(31)
On Pt, log $fO_2 = -9{\cdot}60$, log $fS_2 = -1{\cdot}91$, 17·3 h (22/4/97)					
51·4(1)	14·8(1)	0·0	10·1(1)	24·6(1)	623(72)
52·1(2)	14·5(1)	0·5(1)	9·7(2)	24·3(1)	609(18)
52·4(1)	14·2(2)	0·9(1)	9·6(1)	23·9(2)	663(26)
52·9(2)	14·0(2)	1·4(1)	9·4(1)	23·4(1)	687(30)
54·0(2)	13·0(1)	3·5(1)	8·7(1)	21·8(1)	901(79)
54·9(9)	12·7(2)	3·2(1)	8·7(1)	21·4(4)	796(38)
On Pt, log $fO_2 = -9{\cdot}60$, log $fS_2 = -1{\cdot}91$, 24 h (27/3/97)					
50·6(1)	14·6(1)	0·0	10·1(1)	25·1(1)	625(20)
53·8(1)	13·9(2)	0·2	9·4(1)	23·0(1)	511(24)
57·5(3)	12·1(1)	2·6(1)	8·2(1)	20·0(1)	602(18)
58·2(2)	9·0(1)	11·6(1)	6·2(1)	15·0(1)	2213(30)
62·3(2)	8·0(1)	11·3(1)	5·4(1)	13·1(1)	1951(33)
On Pt, log $fO_2 = -8{\cdot}79$, log $fS_2 = -1{\cdot}91$, 9·3 h (8/3/97)					
50·4(3)	14·9(2)	0·0	10·1(1)	24·7(1)	235(24)
50·2(2)	13·0(1)	6·9(1)	8·8(1)	21·3(2)	685(54)
47·5(2)	10·1(1)	20·0(2)	6·8(1)	16·4(1)	3468(37)
47·4(4)	7·5(1)	29·3(4)	5·1(1)	12·2(1)	7611(36)
51·4(1)	4·6(1)	34·4(1)	3·1(1)	7·5(1)	9832(85)
On $Ir_{80}Fe_{20}$ alloy, log $fO_2 = -9{\cdot}60$, log $fS_2 = -1{\cdot}91$, 68 h (19/3/98)					
49·8(1)	14·7(1)	2·7(1)	9·8(1)	22·7(1)	1048(29)
52·0(2)	13·8(1)	3·8(1)	9·2(1)	21·0(1)	1051(31)
51·7(2)	13·3(1)	4·0(1)	9·1(1)	21·8(1)	1100(17)
55·7(1)	12·1(1)	5·5(1)	8·1(1)	18·4(1)	1170(45)

Runs on Pt wire loops have lost extensive amounts of FeO and should therefore be considered as pseudo-ternary compositions in the system AD eutectic–Fe_2SiO_4–SiO_2.

difference in T. Given the dominance of FeO in controlling C_S, this is again most easily done by plotting C_S as a function of wt % FeO. This has been done in Fig. 19.

Of the 100 experiments of Haughton *et al.* (1974) at 1200°C, 37 were conducted on a single starting composition but with variable FeO content, at various values of fO_2 and fS_2 (their Series I). These data form an array on the log C_S vs FeO diagram parallel to our data at 1400°C, but displaced to lower values of C_S, as expected for the temperature difference. The other 63 experiments (their Series II) were performed at constant fO_2 and fS_2 (namely, $fO_2 = 10^{-9{\cdot}31}$ bars, $fS_2 = 10^{-0{\cdot}98}$ bars), to study the effect of silicate melt composition. These data plot on a significantly shallower slope in the log C_S vs FeO diagram. This is inconsistent not only with our results, but also with their Series I experiments.

There are also major internal inconsistencies in their Series I data. For example, Haughton *et al.* reported three experiments, with the same starting composition, at the same fO_2 and fS_2, and in equilibrium with immiscible FeS-rich sulfide melt (namely runs 4 DF2, 7 DF2 and 7F2 in their appendix). The activity of FeO is constrained to be identical, but FeO contents were 0·88, 1·30 and 4·47 wt %, respectively. This large range cannot be explained by the modest differences in alumina and

Table 14: AD eutectic, replacing MgO with FeO; on Pt, log $fO_2 = -9{\cdot}60$, *log* $fS_2 = -1{\cdot}91$, *12 h (21/3/97)*

SiO_2	Al_2O_3	FeO	MgO	CaO	S (ppm)
50·4(1)	14·7(1)	0	10·2(1)	24·9(1)	629(26)
49·7(2)	20·2(2)	0·27(6)	6·0(1)	24·1(1)	518(29)
50·3(2)	19·9(1)	1·10(11)	4·7(1)	24·5(1)	631(15)
51·4(9)	20·3(4)	1·88(16)	3·1(1)	24·8(1)	585(18)
50·9(1)	19·8(1)	3·59(8)	1·6(1)	24·5(1)	925(20)
52·1(3)	20·5(1)	2·45(9)	0·0(1)	25·2(1)	624(20)

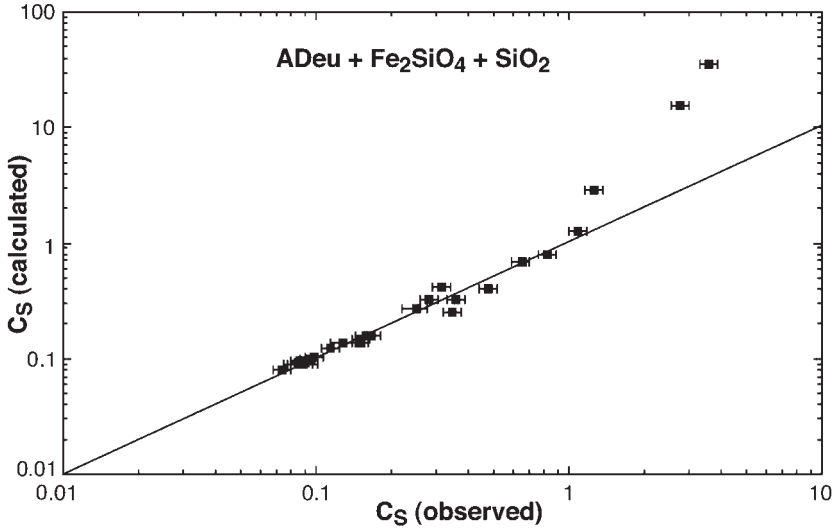

Fig. 15. Test of the model against data for the ternary ADeu–Fe_2SiO_4–SiO_2, which were not used in the calibration. Data from Table 13. It should be noted that the three data points with >20 wt % FeO are not fitted by the model.

other major-element contents in these melts but must be taken as evidence of disequilibrium or other experimental malfunction.

The sheer number of data reported by Haughton *et al.* (1974) has dominated attempts to quantify the role of S in magmatic systems (e.g. Poulson & Ohmoto, 1990; Wallace & Carmichael, 1992; Li & Naldrett, 1993), so our suggestion that their results may be in error is significant. It is our intention to test their results more directly by replicating experiments on their reported compositions at their experimental T of 1200°C.

Attempted replication of some results from Buchanan *et al.* (1983)

In a series of papers, Buchanan, Nolan and coworkers reported the results of sulfur solubility experiments in several CMAS–FeO compositions at T between 1200 and 1400°C (Buchanan & Nolan, 1979; Buchanan *et al.*, 1983; Nolan & Buchanan, 1984). Both the aims and the experimental approach of these papers are similar to those of this study, and indeed we have adopted two of the compositions used by Buchanan & Nolan (DB/3 and PAL 685 in Table 5), to facilitate comparison. This was felt to be important, as the results of Buchanan & Nolan do not follow the Fincham–Richardson relationship ($[S] \propto (fS_2/fO_2)^{1/2}$). Thus the values of C_S calculated from their experiments appear to change as a function of fS_2 (e.g. see Buchanan *et al.*, 1983, fig. 4). Generally, Buchanan & Nolan reported anomalously high [S] at low fS_2, leading to slopes in log [S] vs log fS_2 plots that are far less than the slope of 1/2 required by the Fincham–Richardson relationship. This occurs for all

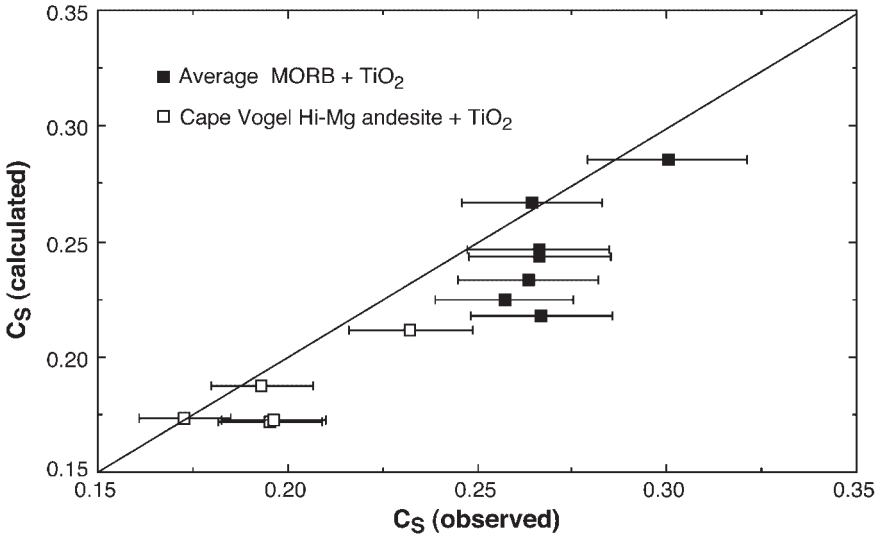

Fig. 16. Test of the model against compositions made by adding TiO_2 to the average MORB and Cape Vogel high-Mg andesite compositions. Data from Table 9.

Table 15: Alkali basalt composition ('Mavbas'—see Mavrogenes & O'Neill, 1999), on Pt and Ir_{80} Fe_{20} alloy

SiO_2	TiO_2	Al_2O_3	FeO	MgO	CaO	Na_2O	K_2O	S (ppm)
'Mavbas' plus $MgSiO_3$ on Pt, log $fO_2 = -9{\cdot}60$, log $fS_2 = -1{\cdot}91$, 16·5 h (7/5/97)								
54·9(3)	2·2(1)	19·4(1)	2·6(1)	7·2(1)	11·8(1)	0·8(1)	1·2(1)	514(25)
55·0(4)	1·9(1)	17·1(1)	2·1(1)	10·6(1)	10·4(1)	0·6(1)	0·9(1)	479(21)
57·2(2)	1·7(1)	15·4(1)	1·7(1)	13·4(1)	9·4(1)	0·5(1)	0·8(1)	393(20)
57·7(3)	1·4(1)	13·1(1)	1·4(1)	17·0(2)	8·1(1)	0·4(1)	0·7(1)	385(34)
57·6(2)	1·2(1)	10·9(1)	2·0(1)	19·8(2)	6·8(1)	0·3(1)	0·6(1)	437(23)
60·1(2)	1·1(1)	9·8(2)	1·1(1)	19·8(1)	6·2(1)	0·5(1)	0·7(1)	345(21)
'Mavbas' on $Ir_{80}Fe_{20}$ alloy, log $fO_2 = -7{\cdot}60$, $fS_2 = 0$, 94 h (8/8/97)								
48·6(3)	1·9(1)	17·1(1)	13·0(3)	6·4(1)	10·4(1)	0·7(1)	1·7(1)	17(14)*
'Mavbas' on $Ir_{80}Fe_{20}$ alloy, log $fO_2 = -7{\cdot}60$, log $fS_2 = -1{\cdot}91$, 70 h (28/8/97)								
49·1(2)	1·9(1)	17·8(1)	12·0(1)	6·6(1)	10·5(1)	1·1(1)	1·3(1)	230(18)
'Mavbas' on $Ir_{80}Fe_{20}$ alloy, log $fO_2 = -7{\cdot}60$, log $fS_2 = -1{\cdot}02$, 7 h (4/9/97)								
48·9(2)	1·9(1)	17·1(1)	11·8(2)	6·4(1)	10·4(1)	1·9(1)	1·3(1)	856(27)

Runs on Pt have suffered extensive Fe loss. All runs have also lost alkalis (Na and K).
*Test of $Ir_{80}Fe_{20}$ alloy. Sulfur content should of course be zero.

their sulfide-undersaturated compositions throughout the T range of their work (1200–1400°C).

In contrast, our results on the Buchanan & Nolan compositions (DB/3D and PAL/D) do obey the Fincham–Richardson relationship when we vary fO_2 at constant fS_2 (Fig. 5). However, at fO_2 of $10^{-10{\cdot}28}$ bars, which we chose to keep constant while varying fS_2, these compositions are saturated with immiscible FeS-rich sulfide melt, and hence the FeO content in the silicate melt also varies. This change of composition foils the simple, direct test of the Fincham–Richardson relationship vs fS_2. Therefore, to test the relationship, two additional experiments were performed at sulfide-undersaturated conditions, replicating two Buchanan *et al.* (1983) experiments at 1400°C. We used exactly the same CO–CO_2–SO_2 gas flow rates as Buchanan *et al.*

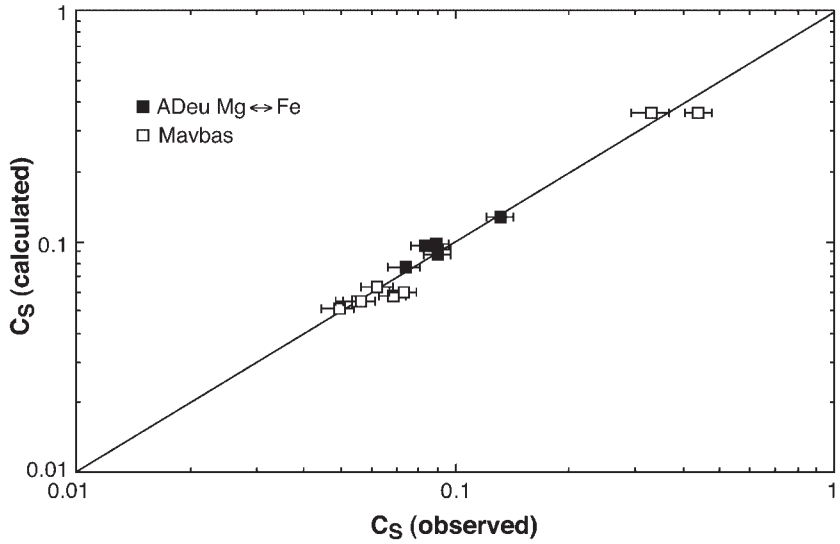

Fig. 17. Test of the model against various other compositions not used for data fitting (Tables 14 and 15).

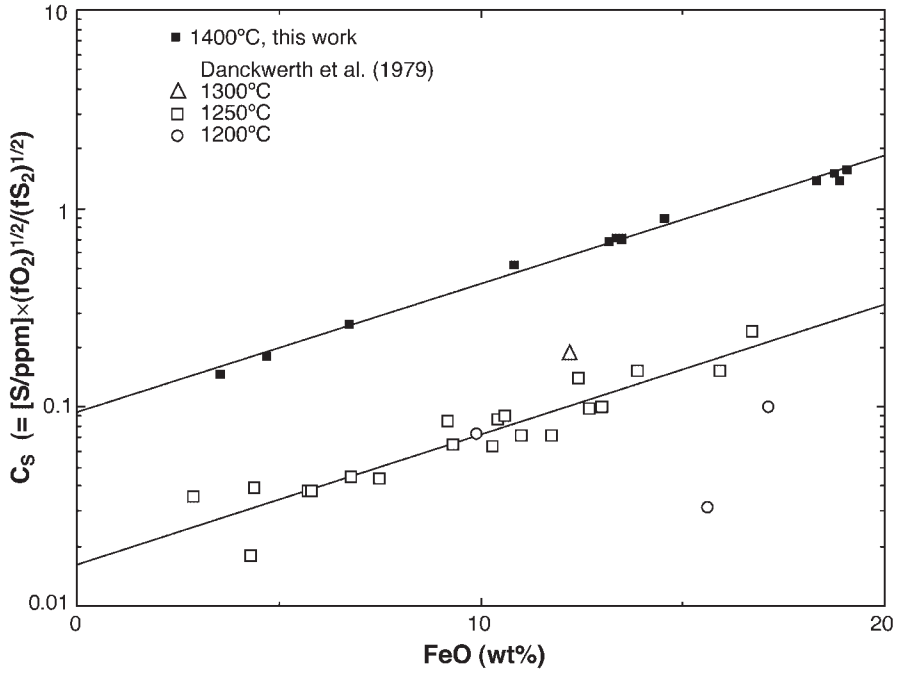

Fig. 18. Comparison of our results on the high-Ti mare basalt composition (at 1400°C) vs those of Danckwerth *et al.* (1979), mainly at 1250°C. The latter form a linear array with an identical slope, but displaced to lower values of log C_S.

(1983). The results are given in Table 16, along with the original results from Buchanan *et al.* (1983), and compared in Fig. 20. There are clearly large differences in the results. Most importantly, our results show [S] $\propto$ $(fS_2)^{1/2}$, in accordance with the Fincham–Richardson relationship.

DISCUSSION

Sulfur content at sulfide saturation (SCSS)

For most geological applications, the main question of interest concerning S solubility in magmas is at what point the magma becomes saturated in immiscible

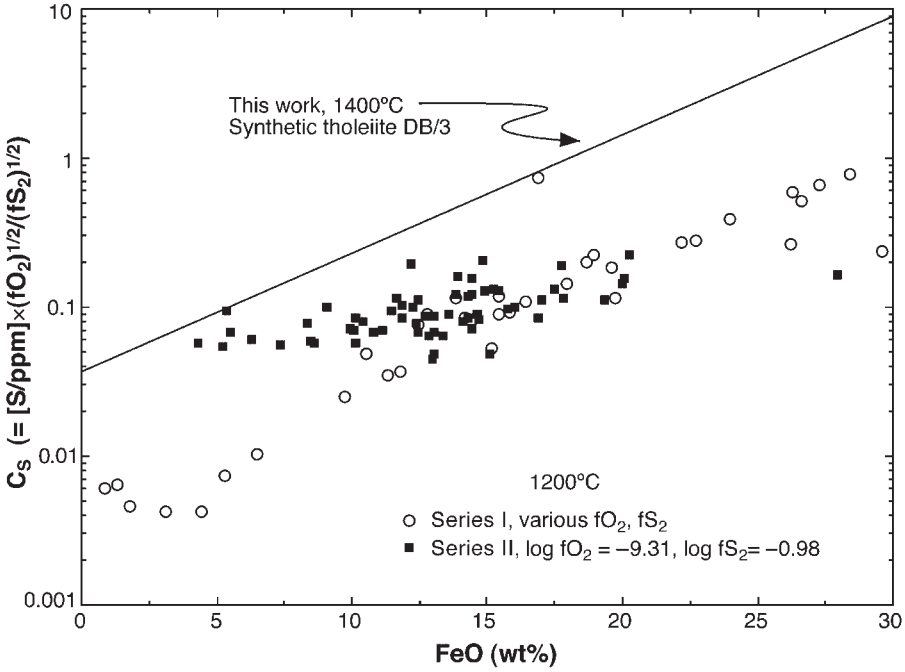

Fig. 19. Sulfide capacities (C_S) from the experiments of Haughton *et al.* (1974), at 1200°C. For comparison, our results on one composition, the synthetic tholeiite DB/3, at 1400°C are plotted. Series I (of Haughton *et al.*, 1974) defines a parallel trend displaced to lower temperature, as expected (see also Fig. 18); but their Series II data (all at the same fO_2 and fS_2) display a different, shallower slope in log C_S vs FeO space.

Table 16: Experiments replicating Buchanan et al. *(1983) on the relationship between sulfide solubility and* fS_2*, at 1400°C*

Oxide	AD eutectic	PAL/D this study	PAL/D B *et al.* (1983)	DB/3D this study	DB/3D B *et al.* (1983)
log $fO_2 = -8{\cdot}50$, *log* $fS_2 = -3{\cdot}50$, *48 h (12/7/99)*					
SiO_2	50·51(24)	58·13(28)	59·34(32)	48·60(40)	48·73(30)
Al_2O_3	15·15(15)	13·10(3)	13·05(20)	15·16(11)	14·97(11)
CaO	24·08(13)	8·97(6)	8·85(10)	8·55(6)	8·35(9)
MgO	10·46(9)	4·23(7)	4·16(9)	11·30(5)	11·28(14)
FeO	—	14·62(6)	14·41(25)	16·23(11)	16·23(19)
S (ppm)	54(11)	184(17)	850	232(20)	1250
	[28]*		(780–960)		(1090–1360)
log $fO_2 = -8{\cdot}50$, *log* $fS_2 = -2{\cdot}00$, *24 h (19/7/99)*					
SiO_2	50·45(16)	58·48(35)	59·45(36)	48·27(22)	48·72(30)
Al_2O_3	15·19(12)	13·11(13)	13·16(12)	15·06(12)	15·12(12)
CaO	24·11(8)	8·93(2)	8·90(11)	8·45(5)	8·35(10)
MgO	10·60(10)	4·20(4)	4·23(11)	11·31(4)	11·36(11)
FeO	—	14·51(18)	14·18(18)	16·34(7)	16·19(17)
S (ppm)	189(13)	843(23)	1170	1207(25)	1790
	[155]*		(1080–1250)		(1630–1930)

*Calculated using $C_S = 0{\cdot}87$ for ADeu composition.

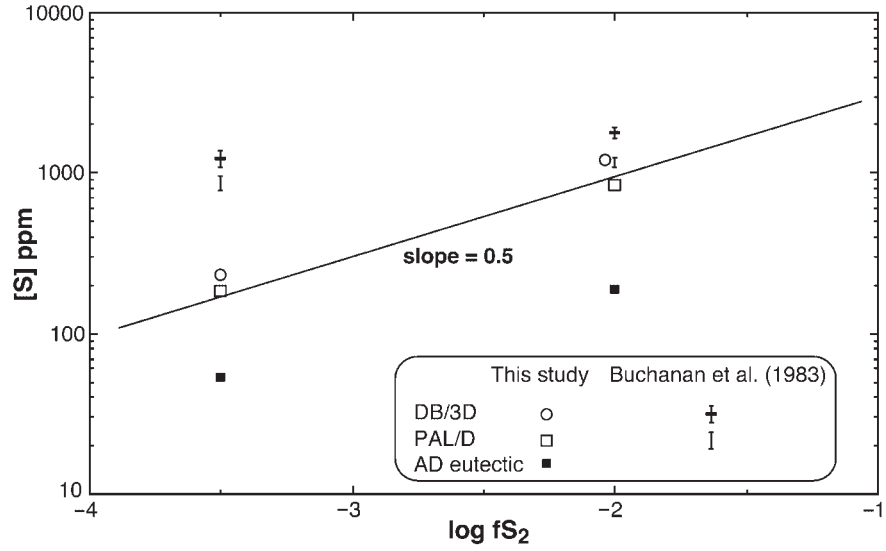

Fig. 20. Attempted replication of the experiments of Buchanan *et al.* (1983) (see Table 16). All samples are undersaturated in FeS, hence silicate compositions remain constant. A line with the theoretical slope of 0·5 (positioned arbitrarily) is shown. The results of Buchanan *et al.* plot on an almost horizontal slope.

sulfide. Many of the experiments on Fe-containing compositions in this study produced an immiscible FeS-rich sulfide melt, and therefore bear directly on this question.

The equilibrium between a silicate melt and an FeS-rich immiscible sulfide phase can be described by the reaction

$$\underset{\text{silicate melt}}{\text{FeO}} + \tfrac{1}{2}\text{S}_2 = \underset{\text{sulfide melt}}{\text{FeS}} + \tfrac{1}{2}\text{O}_2 \qquad (22)$$

for which

$$-\Delta G^\circ\,(22)/RT = \ln a_{\text{FeS}}^{\text{sulfide}} - \ln a_{\text{FeO}}^{\text{silicate}} + \tfrac{1}{2}\ln (fO_2/fS_2). \qquad (23)$$

Substituting equation (2) into (23) to eliminate fO_2 and fS_2 gives

$$\ln [\text{S}]_{\text{SCSS}} = \Delta G^\circ\,(22)/RT + \ln C_{\text{S}} + \ln a_{\text{FeS}}^{\text{sulfide}} - \ln a_{\text{FeO}}^{\text{silicate}} \qquad (24)$$

where $[\text{S}]_{\text{SCSS}}$ is the 'sulfur content at sulfide saturation', a term introduced by Shima & Naldrett (1975). Thermodynamic data for liquid FeO and FeS from O'Neill & Eggins (2002) and Barin *et al.* (1989) respectively, give

$$\Delta G^\circ(22) = 122175 - 80{\cdot}280\,T + 8{\cdot}474\,T\ln T \text{ J mol}^{-1}. \qquad (25)$$

Sulfur saturation therefore depends on the amount of S in the magma, the major-element composition of the magma, the composition of the immiscible sulfide, and T and P. As pointed out by Mavrogenes & O'Neill (1999), the SCSS of a magma is independent of fO_2 and fS_2, provided that the silicate melt composition is kept constant (no gain or loss of FeO, for example), except for the effects that fO_2 and fS_2 have on the composition of the immiscible sulfide, i.e. on $a_{\text{FeS}}^{\text{sulfide}}$. For example, at very low fO_2 the composition of the immiscible sulfide has Fe/S >1 (i.e. solution of Fe in FeS), lowering $a_{\text{FeS}}^{\text{sulfide}}$ and causing SCSS to fall, as experimentally demonstrated by Mavrogenes & O'Neill (1999). But for all fO_2 conditions used in this study, we assume that the immiscible sulfide melt produced in our experiments is effectively pure FeS, hence $a_{\text{FeS}}^{\text{sulfide}} = 1$. In detail, there may be small variations in $a_{\text{FeS}}^{\text{sulfide}}$ as a result of dissolved oxygen in the sulfide melt, and deviations from atomic Fe/(S + O) ratios of unity (e.g. Kress, 1997). However, preserving the compositions of sulfide melts during quenching requires extremely fast quench rates (Kress, 1997), which were not attempted in this study. Probably in consequence, electron microprobe analysis of the quenched immiscible sulfide gave >99% FeS in all experiments. In particular, we were not able to find any quenched iron oxide phases associated with the sulfide. Some natural magmas, including those of economic interest, contain chalcophile elements such as Ni, Co and Cu, in sufficient abundances to reduce $a_{\text{FeS}}^{\text{sulfide}}$ significantly.

The interesting feature of equation (24) is that it shows that the SCSS of a silicate melt depends on its FeO content from two different terms, namely $\ln C_{\text{S}}$, which is dominated by its dependence on X_{Fe}, and $a_{\text{FeO}}^{\text{silicate}}$. This latter term may be split up into two parts:

$$\ln a_{\text{FeO}}^{\text{silicate}} = \ln X_{\text{Fe}} + \ln \gamma_{\text{Fe}} \qquad (26)$$

where γ_{Fe} is the activity coefficient of FeO in the silicate melt. Experimental evidence shows that γ_{Fe} is reasonably close to unity for a wide variety of silicate melt compositions (e.g. Roeder, 1974; Doyle & Naldrett, 1986; Doyle, 1988; O'Neill & Eggins, 2002). In detail, γ_{Fe} at low X_{Fe} is usually slightly greater than unity for most compositions in the system CMAS–FeO at 1400°C, when referred to a standard state of liquid FeO. For most of the compositions measured by O'Neill & Eggins (2002), $1{\cdot}1 < \gamma_{Fe} < 1{\cdot}5$. However, γ_{Fe} becomes less than unity for compositions high in TiO_2 (Roeder, 1974; Doyle, 1989; O'Neill & Eggins, 2002).

For the compositions along the binary joins between 'Matrix' (the FeO-free end-member) and FeO that are produced in our experiments on the 'Fe6' starting compositions (Table 4), equation (24) then becomes

$$\ln[S]_{SCSS} = \Delta G^\circ(22)/RT + A_0 + (1 - X_{Fe})\sum_{M \neq Fe} A_M X_M^\circ + B_{Fe\text{-}Ti} X_{Ti}^\circ (1 - X_{Fe}) X_{Fe} + A_{Fe} X_{Fe} - \ln X_{Fe} - \ln \gamma_{Fe}. \quad (27)$$

Here the parameters X_M° are the mole fractions of the 'Matrix' compositions, which are given in Table 5. The $\ln a_{FeS}^{sulfide}$ term is omitted for this exercise, as discussed above. Because $\gamma_{Fe} \rightarrow 1$ as $X_{Fe} \rightarrow 1$ by definition, the term in $\ln \gamma_{Fe}$ is also generally a function of X_{Fe}. However, as accurate values of γ_{Fe} are not available for the 'Fe6' compositions of interest here, we will adopt the simplifying approximation that γ_{Fe} is unity. Equations (24) and (27) of course apply only to equilibrium with FeS-rich sulfide, and are not defined for Fe-free systems. Because $0 < X_{Fe} < 1$, the $A_{Fe}X_{Fe}$ term has a positive sign with a positive slope vs FeO, and dominates at high X_{Fe}, whereas the $-\ln X_{Fe}$ term has a positive sign, a negative slope vs FeO, and dominates at low X_{Fe}. The net result is that $[S]_{SCSS}$ should show an asymmetric U-shaped dependence on X_{Fe}. To illustrate this, we have fitted the S solubilities from the FeS-saturated 'Fe6' samples to equation (27), treating only the term in $\Delta G^\circ(22)/RT$ as an unknown. The results of the fitting are given in Table 17, and illustrated in Fig. 21. All five compositions with minor TiO_2 give essentially identical values of $\Delta G^\circ(22)/RT$, of $6{\cdot}35 \pm 0{\cdot}02$, which when compared with the theoretical value expected from equation (25) of 6·69 at 1400°C, imply γ_{Fe} of $\sim 1{\cdot}4$, in good agreement with measurements on similar compositions in the CMAS system (O'Neill & Eggins, 2002). The higher calculated value of $\Delta G^\circ(22)/RT$ for the high-Ti mare basalt series (6·72) is consistent with the expected lower value of γ_{Fe} for this composition.

However, the fits to some compositions, particularly the synthetic tholeiite PAL 685, are not good. In truth, our present experimental data do not really extend to low enough values of X_{Fe} to demonstrate unambiguously the upturn expected in $[S]_{SCSS}$. The required combination of low fO_2 and high fS_2 to produce low-FeO silicate melts in equilibrium with FeS melt cannot be attained in atmospheric-pressure experiments using CO–CO_2–SO_2 gas mixtures (as may be seen from the gas mixtures used for the experiments, which are given in Table 3). In any case, at lower fO_2, the increasing solubility of Fe in the FeS melt would produce significant errors in the assumption that $a_{FeS}^{sulfide} = 1$. Nevertheless, logic dictates that there must be an upturn, as saturation with FeS-rich sulfide must become more difficult as the Fe content of the system decreases towards zero.

Significance of the A_M terms in the equation for C_S

The derivation of the equation relating C_S to composition derived in the section on 'Thermodynamic theory' [equation (17)] identifies the coefficients A_M with the difference in the free energies of formation of M_zS and M_zO, i.e.

$$A_M = (\mu_{M_zO}^\circ - \mu_{M_zS}^\circ)/RT - \text{constant}. \quad (19)$$

This shows that the reason why Fe has such a great influence on C_S is simply that FeS is rather stable, thermodynamically, compared with FeO. This simple observation is of great importance, as it goes to the heart of why approaches that do not take into account the specific identity of cation–anion interactions are bound to fail. These approaches include those based on optical basicity, or the ratio of non-bridging oxygens to tetrahedrally co-ordinated cations (often designated NBO/T). A feature of such approaches is that they seek to explain a wide range of silicate melt properties through one or a few chosen parameters; hence a convenient collective term for them might be 'universal melt descriptors'. We discuss the inadequacies of this type of approach later, but first we will discuss the deficiencies in our own model.

Thermochemical data (e.g. Barin *et al.*, 1989) show that the relationship of equation (19) is not correct in detail, and does not supply quantitative estimates of the values of the A_M terms. Nor does it predict the relative values of these terms among cations completely correctly. For example, for the divalent cations Ca, Mg and Fe, the thermochemical data for $(\mu_{M_zO}^\circ - \mu_{M_zS}^\circ)$ predict that $A_{Ca} > A_{Fe} \gg A_{Mg}$, whereas empirically we find $A_{Fe} \gg A_{Ca} > A_{Mg}$.

In any case, many studies of silicate melts (or strictly speaking, their quenched glasses) have shown that the number of O^{2-} anions in compositions richer in silica than the orthosilicate ratio is negligibly small (e.g. Mysen, 1988). All the melt compositions investigated in this study lie in this category. Rather, such melts are better modelled as consisting of a range of polymer units, whose general

Table 17: Results of fitting the sulfur contents at sulfide saturation (SCSS) for 'Fe6' data to equation (27), assuming $\gamma_{Fe} = 1$

Composition	$\frac{\Delta G^\circ(22)}{RT}$	χ^2_ν	Number of data
Average MORB	6·34(2)	0·61	8
Olivine tholeiite	6·43(2)	0·95	8
Synthetic tholeiite PAL 685	6·38(2)	10·4	9
Synthetic tholeiite DB/3	6·36(2)	0·57	8
Cape Vogel andesite	6·35(2)	5·75	8
High-Ti mare basalt	6·74(2)	3·55	9

Data were weighted assuming an error in analysed S of 5% or as observed from the electron microprobe analyses (Table 4), whichever is larger.

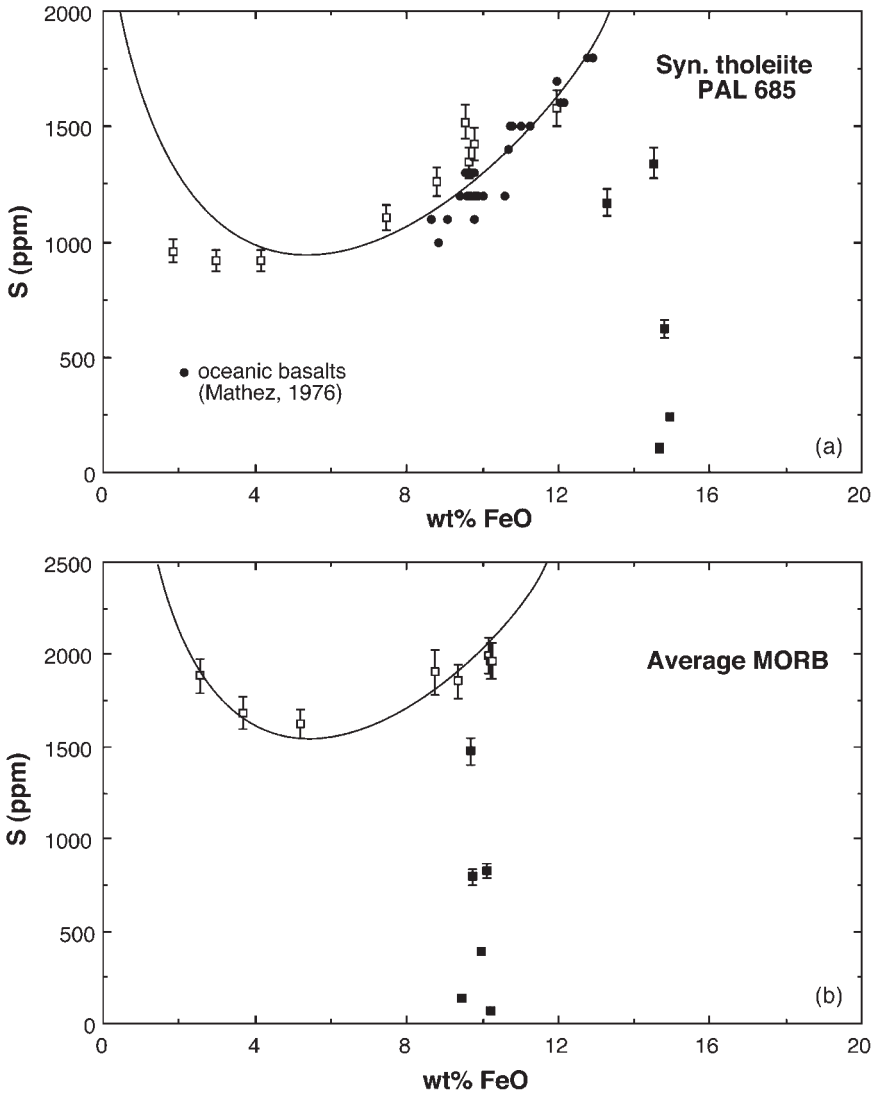

Fig. 21.

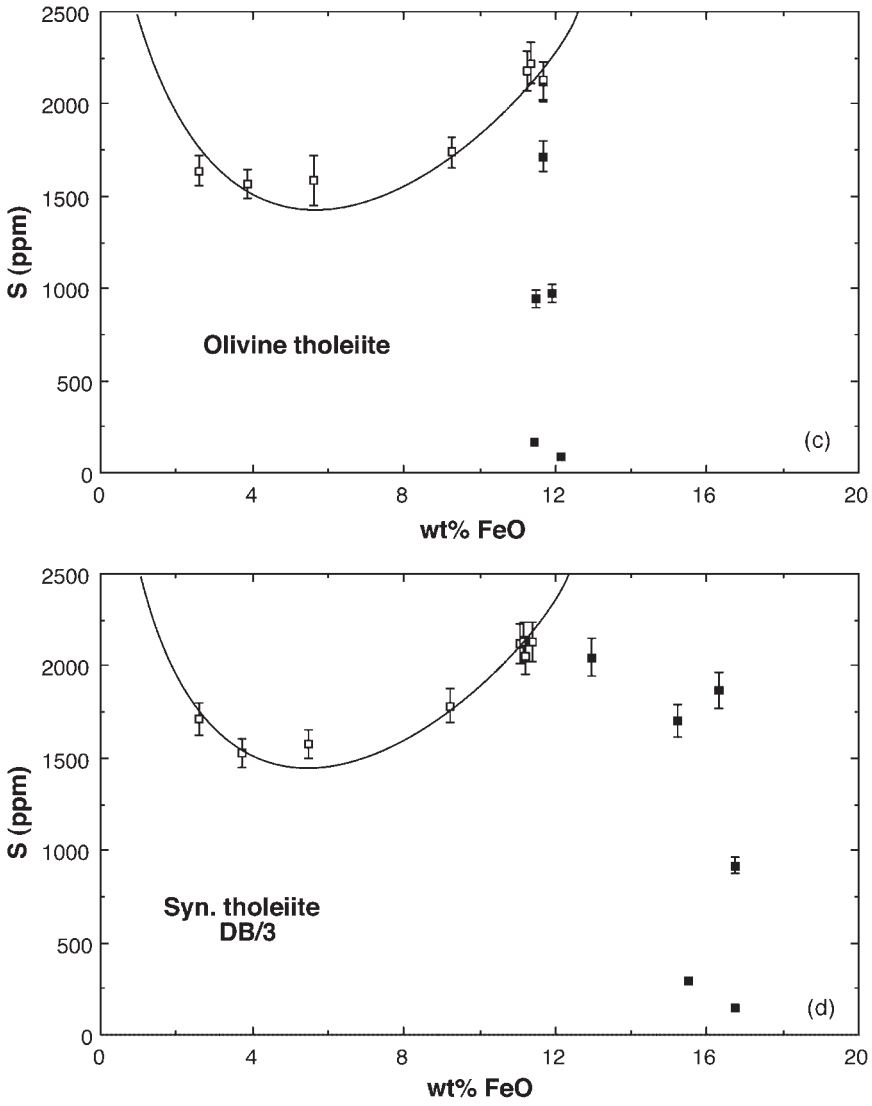

Fig. 21.

formula may be written $(SiO_{4-y/2})^{(4-y)-}$, with $0 \leq y \leq 4$. When $y = 0$, the unit is the orthosilicate unit SiO_4^{4-}, in which Si is co-ordinated by four non-bridging oxygens. At the opposite extreme, $y = 4$ gives the fully polymerized silicate unit SiO_2^0, with no non-bridging oxygens. Thus the hypothetical degree of polymerization of a silicate melt can be described by the ratio of non-bridging oxygens to tetrahedral cations, NBO/T, which ranges from four for an orthosilicate composition melt such as Mg_2SiO_4 to zero for a completely polymerized melt such as pure SiO_2 or $NaAlSi_3O_8$. Melts more basic than the orthosilicate composition must indeed have free O^{2-} anions, but these melts have NBO/T >4 and are of limited importance geologically. A melt of a pure simple oxide such as MgO has NBO/T of infinity. This structural view of silicate melts is reflected in the choice of components with mineral-like stoichiometries to model their thermodynamic properties (e.g. Ghiorso & Sack, 1995).

This all suggests that, as the next increment of sophistication, the Fincham–Richardson reaction could be modified for natural silicate melts to

$$S^{2-} + \tfrac{1}{2}\,O_2 + \tfrac{1}{2}\,SiO_2^0 = \tfrac{1}{2}\,SiO_4^{4-} + \tfrac{1}{2}\,S_2. \qquad (28)$$

As a simplifying approximation, we have ignored intermediate polymer units. Hence

$$\ln C_S = \ln[S] + \tfrac{1}{2}\ln(fO_2/fS_2) + \tfrac{1}{2}\ln(X_{SiO_2^0}/X_{SiO_4^{4-}}). \qquad (29)$$

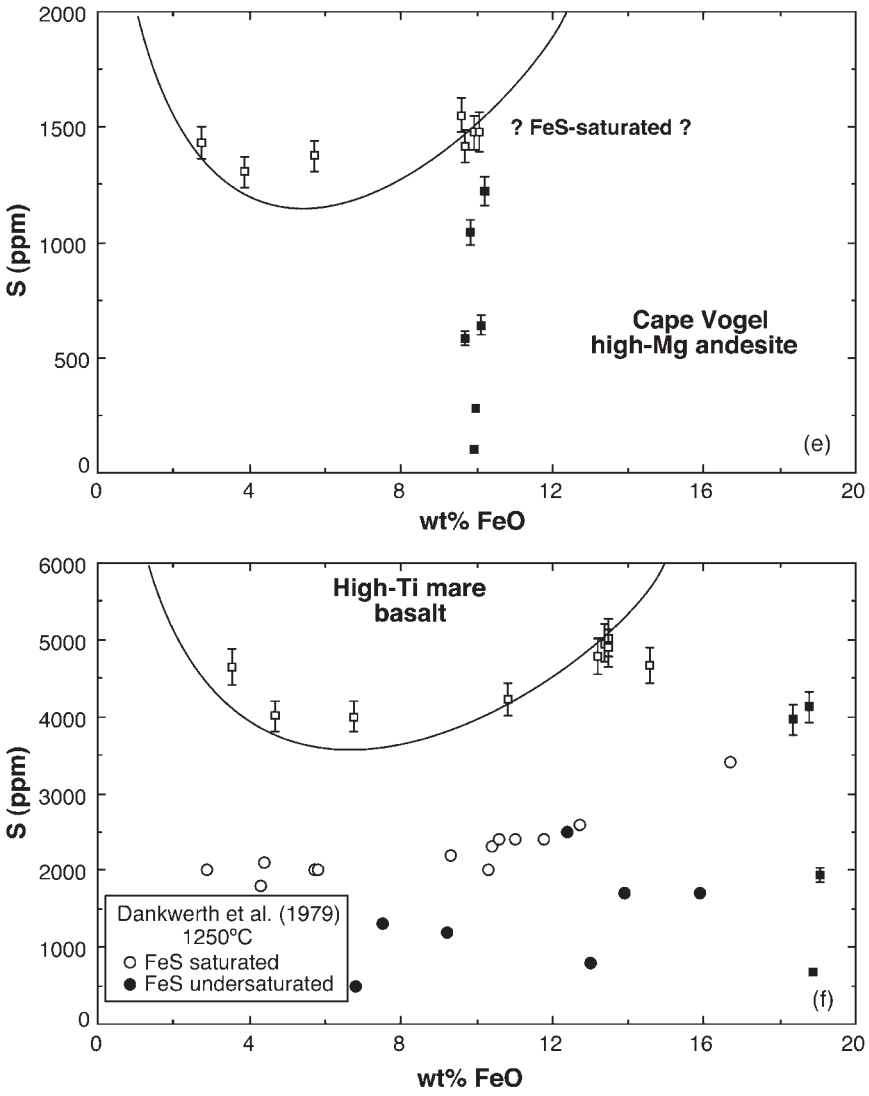

Fig. 21. Sulfur content at sulfide saturation (SCSS) for 'Fe6' compositions, as a function of FeO content of the silicate melt. Open symbols are for experiments saturated with immiscible FeS-rich melt, which are expected theoretically to lie on an asymmetrical U-shaped curve [see equations (24) and (26)]. FeS-undersaturated experiments (■) are constrained to lie below this curve. In (a) the observed S contents of natural oceanic basaltic glasses are also plotted (Mathez, 1976). In (f) the data of Dankwerth *et al.* (1979) on the sample binary join at 1250°C are also plotted.

This reaction still requires the dependence of C_S on $(fO_2/fS_2)^{1/2}$ that is seen in the experiments, but suggests that C_S should also depend on the ratio of polymerized silica units to orthosilicate units, i.e. effectively NBO/T. By analogy with the thermodynamic derivation of the compositional dependence of C_S given above for simple oxide components, the coefficients A_M for this approach would be expected to be proportional to $(1/2\mu^\circ_{M_2SiO_4} - \mu^\circ_{M_2S})$ rather than to $(\mu^\circ_{M_2O} - \mu^\circ_{M_2S})$. This is qualitatively in accord with the observation that $A_{Fe} \gg A_{Ca} > A_{Mg}$. The reason that the A_{Fe} term is so large is not only the relatively large thermodynamic stability of FeS, but also the relatively low stability of Fe_2SiO_4 compared with its oxide components FeO and SiO_2.

As a first step to test this approach, we examined the residuals from the regression of our data to equation (19) against NBO/T. No correlation is observed. Second, we included the term $1/2\ln(X_{SiO_2^0}/X_{SiO_4^{4-}})$ in the regression, using various strategies to calculate $X_{SiO_2^0}/X_{SiO_4^{4-}}$ and ignoring the possibility of intermediate polymer units. The ambiguity comes from how Al and to a lesser extent Ti are assigned in the polymer model. For example, Al could be treated as a simple cation Al^{3+} (mixing on the cation sublattice with Ca^{2+}, Mg^{2+}, Fe^{2+}, Na^+, etc.), or

as an isolated octahedral or tetrahedral unit equivalent to the orthosilicate unit, AlO_4^{5-}, or as a fully polymerized tetrahedral unit, AlO_2^-. The way in which mole fractions of other cations are defined depends on such assignments, and is therefore also equivocal. Clearly, there is a wide range of possible formulations even though the conceptual basis of this approach is very simplified. The important point is that nothing we tried could achieve as good an empirical fit as the simple-oxide approach of equations (17) and (20). Rather surprisingly, the better results came from models in which Al was treated as a simple Al^{3+} cation.

It is probable that further theoretical work will result in more sophisticated models that fit the sulfur solubility data better than the naive model used here. In anticipation of such progress, we have made a point in this paper of giving all our experimental data on equilibrium S solubilities in full.

Comparison with optical basicity models

Optical basicity is 'a measure of the donor power of the oxides . . . [that] has been used to relate slag composition to sulfur capacities' (Young *et al.*, 1992). The concept is closely related to Pauling's scale of electronegativity (Duffy, 1993). Optical basicities were originally quantified through 'spectroscopic measurements of the shift of frequency in the UV region of a selected absorption band of a doping agent (Bi^{3+}, Pb^{2+} or Tl^+) caused by the electron donor environment of a glass made from the oxide system being investigated' (Young *et al.*, 1992). Such measurements are not possible for glasses containing transition element oxides, and instead various empirical methods have been developed to improvise fictive 'optical basicity' values directly from the chemical analysis of a glass (Duffy & Ingram, 1975; Sosinsky & Somerville, 1986; Young *et al.*, 1992). Thus Sosinsky & Somerville (1986) and Young *et al.* (1992) defined their fictive optical basicity Λ as

$$\Lambda = \sum_M \Lambda_M X_M^\Lambda \tag{30}$$

where Λ_M are the values of optical basicity assigned to each oxide component. In the formulation of Young *et al.* (1992), $\Lambda_{Si} = 0{\cdot}46$, $\Lambda_{Al} = 0{\cdot}60$, $\Lambda_{Mg} = 0{\cdot}78$, $\Lambda_{Ca} = \Lambda_{Fe} = 1{\cdot}00$, $\Lambda_{Na} = 1{\cdot}15$, and $\Lambda_K = 1{\cdot}4$. The X_M^Λ are 'equivalent cation fractions', and are given the distinguishing superscript as they are defined somewhat differently from any customary way of defining mole fractions, including that adopted here (see Sosinksky & Somerville, 1986). For example, in the system CaO–Al_2O_3–SiO_2:

$$X_{Ca}^\Lambda = \frac{\mathcal{N}_{CaO}}{\mathcal{N}_{CaO} + 3\mathcal{N}_{Al_2O_3} + 2\mathcal{N}_{SiO_2}} \tag{31a}$$

$$X_{Al}^\Lambda = \frac{3\mathcal{N}_{Al_2O_3}}{\mathcal{N}_{CaO} + 3\mathcal{N}_{Al_2O_3} + 2\mathcal{N}_{SiO_2}} \tag{31b}$$

$$X_{Si}^\Lambda = \frac{2\mathcal{N}_{SiO_2}}{\mathcal{N}_{CaO} + 3\mathcal{N}_{Al_2O_3} + 2\mathcal{N}_{SiO_2}}. \tag{31c}$$

Young *et al.* (1992) gave an empirical expression for the sulfide capacity as a function of optical basicity, calibrated against an extensive compilation of experimental results from the metallurgical literature, for melts with $\Lambda < 0{\cdot}8$ (which covers all the compositions used in this study):

$$\log C_S = -13{\cdot}913 + 42{\cdot}84\Lambda - 23{\cdot}82\Lambda^2 - (11710/T) - 0{\cdot}02223c_{SiO_2} - 0{\cdot}02275c_{Al_2O_3}. \tag{32}$$

We have applied this expression to the 154 data used in fitting our own model. The results are shown in Fig. 22. Obviously the model does not reproduce the experimental data well. In fact, for the terrestrial Fe-bearing compositions that are of most practical interest, the discrepancy is over an order of magnitude.

Part of the reason for this is that the 'optical basicity' model is calibrated against slag compositions that tend to be more basic than the geologically relevant melt compositions used in this study. However, the main reason is the failure of the optical basicity approach to handle the strong affinity that the FeO component in the silicate melt has for sulfide.

CONCLUSIONS

The C_S of a natural basaltic silicate melt depends mainly on its FeO content. In fact, the FeO content so dominates C_S that the other major-element oxide components are largely irrelevant when computing C_S for typical terrestrial basaltic compositions, and a good approximation may be achieved by using a simple empirical expression:

$$C_S(\text{ppm}) = 0{\cdot}0003(100 - c_{FeO}) \exp\{0{\cdot}21c_{FeO}\} \tag{33}$$

where c_{FeO} is the concentration of FeO in the melt in weight percent [see equation (5) and Table 6]. This equation is of course only valid at reasonably low oxygen fugacities where S dissolves in the melt as S^{2-} and most of the Fe occurs as Fe^{2+}.

The overarching importance of FeO in controlling S solubilities may explain the different approaches to the modelling of C_S as a function of composition that the metallurgical and geological scientific communities have used. The slag compositions of most interest to metallurgists are either very poor in FeO or, more rarely, very rich in FeO (i.e. the FeO–SiO_2 binary), but do not

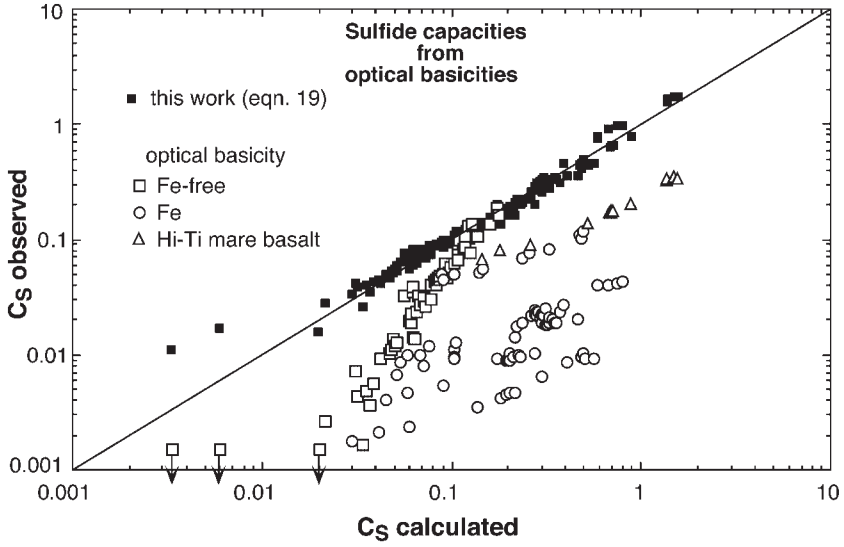

Fig. 22. Calculated sulfide capacities from the 'optical basicity' model of Young *et al.* (1992).

include compositions with intermediate values of FeO comparable with those found in natural silicate magmas. Nor does the metallurgical literature include any work in which the effect of FeO is studied systematically by adding it to originally FeO-poor compositions, as in this study. The result is that metallurgists have sought to model C_S in terms of 'universal melt descriptors' such as optical basicity (e.g. Young *et al.*, 1992), whereas geologists have emphasized simply the FeO content. The data of this study show unambiguously that the optical basicity and related approaches are misguided, as substituting Fe for Mg or Ca on a one-to-one molar basis makes negligible difference to optical basicity (or no difference at all to other universal melt descriptors such as NBO/T), whereas it has a huge effect on C_S. It is the identity of the cations that is important in controlling C_S. 'Carbonate capacities' or 'phosphate capacities', describing the solubilities of CO_3^{2-} and PO_4^{3-}, can be defined in a similar way to the sulfide capacities, but, because $FeCO_3$ and Fe-phosphates are not particularly stable thermodynamically (e.g. relative to $CaCO_3$ and Ca-phosphates), we would not expect the FeO content of the silicate melt to have such a strong influence on them. Rather, from the same thermodynamic reasoning as used to derive our equation for C_S as a function of melt composition, we would expect that CaO and alkali oxides (Na_2O and K_2O) should greatly outweigh FeO in increasing carbonate and phosphate capacities.

An equation describing the sulfur content at sulfide saturation (SCSS) of a silicate melt is obtained by combining three equations: (1) the definition of C_S [equation (2)]; (2) the equilibrium between FeO in the silicate melt and FeS in immiscible sulfide melt [equation (23)]; (3) the compositional dependence of C_S. This equation [equation (27)] predicts that SCSS should show an asymmetric U-shaped dependence on the FeO content of the silicate melt. Experiments that produced immiscible FeS melt conform reasonably well with this expectation (Fig. 21). SCSS also depends on T [illustrated here in Fig. 21f, where our results on the high-Ti mare basalt at 1400°C may be compared with the earlier work of Danckwerth *et al.* (1979) on the same compositions at 1250°C], and on P (Mavrogenes & O'Neill, 1999), but does not, we emphasize, depend on fS_2 or fO_2 (provided that the immiscible sulfide is nearly stoichiometric FeS). It is true that fS_2 and fO_2 must vary in inverse proportion to each other along the sulfide saturation surface in T–P–fS_2–fO_2–composition space [equations (22) and (23)]. The point is that, whereas the location of the sulfide saturation surface depends on $(fO_2/fS_2)^{1/2}$, the actual value of SCSS on this surface depends only on T, P and the composition of the silicate and sulfide melts [equation (24)]. If this fairly simple truth has evaded previous discussion of sulfide equilibria in basaltic systems, this may be because much of the previous theoretical ('thermodynamic') treatment has been fallacious. It is important to point this out, as those unfamiliar with the thermodynamic treatment of phase equilibria may become confused if they consult previous work without a great deal of scepticism. The implications of the present observations for the deposition of sulfide ores will be discussed elsewhere (Mavrogenes & O'Neill, in preparation).

It has long been inferred from the sulfur contents of MORB glasses that SCSS increases with increasing FeO

in natural magmas (Mathez, 1976; Wallace & Carmichael, 1992). The data from Mathez (1976) are plotted for comparison with our experimental results in Fig. 21a. The linear trend of the Mathez data is reproduced well by the experimental curve, but Fig. 21a also shows that this linear trend is in fact expected only over a limited range of FeO contents. It should be noted, also, that the oceanic basaltic glasses are likely to record equilibrium between melt and immiscible sulfide from a rather lower temperature than the 1400°C of the experiments.

The extraordinary nature of this increase of S with increasing FeO has perhaps not been appreciated fully. It is extraordinary because the 'law of mass action' (a simplified and admittedly primitive precursor to the concept of the equilibrium constant in chemical thermodynamics) would predict that dissolved S in equilibrium with immiscible FeS-rich sulfide should decrease with increasing FeO. This may be seen by considering the reaction

$$\underset{\text{sulfide melt}}{\text{FeS}} + \underset{\text{silicate melt}}{\text{O}^{2-}} = \underset{\text{silicate melt}}{\text{FeO}} + \underset{\text{silicate melt}}{\text{S}^{2-}} \qquad (34)$$

for which, if the sulfide melt is pure FeS:

$$\kappa(34) = [\text{FeO}][\text{S}^{2-}]/[\text{O}^{2-}]. \qquad (35)$$

[It should be noted that $\kappa(34)$ is not a thermodynamic equilibrium constant, as charged species such as O^{2-} and S^{2-} are not proper thermodynamic components, because they cannot be varied independently.] Assuming $[O^{2-}]$ is constant [compare the assumption in the Fincham–Richardson model, as in equation (2)], then a constant $\kappa(34)$ would imply that $[S^{2-}] \propto 1/[\text{FeO}]$, i.e. that S in a silicate melt should decrease as FeO increases. That this does not happen in natural compositions follows from the enormous effect that FeO has on C_S.

ACKNOWLEDGEMENTS

We thank Nick Ware for the EMP routine for analysing S by WDS, and many helpers for carrying out the analyses, both EDS and WDS, on our EMP, which dates from the pre-automatic era. Prominent among these helpers was Dean Scott, who also assisted by making many of the starting compositions and loading these onto wire loops. Mike Shelley kept the gas plumbing and the mass flow controllers in good shape, and also undertook the checking of the flow-rate calibrations as required. J.A.M. acknowledges support from Western Mining Corporation during the early stages of this work. Ed Mathez and Roger Powell are thanked for helpful reviews, and Richard Arculus for editorial handling.

REFERENCES

Barin, I., Sauert, F., Schultze-Rhonhof, E. & Sheng, W. S. (1989). *Thermochemical Data of Pure Substances, Part I and Part II*. Weinheim: VCH, pp. 1–1739.

Borisov, A. & Jones, J. H. (1999). An evaluation of Re, as an alternative to Pt, for the 1 bar loop technique: an experimental study at 1400°C. *American Mineralogist* **84**, 1528–1534.

Brooker, R. A., Kohn, S. C., Holloway, J. R. & McMillan, P. F. (2001*a*). Structural controls on the solubility of CO_2 in silicate melts. Part I: bulk solubility data. *Chemical Geology* **174**, 225–239.

Brooker, R. A., Kohn, S. C., Holloway, J. R. & McMillan, P. F. (2001*b*). Structural controls on the solubility of CO_2 in silicate melts. Part II: IR characteristics of carbonate groups in silicate glasses. *Chemical Geology* **174**, 241–254.

Buchanan, D. L. & Nolan, J. (1979). Solubility of sulfur and sulfide immiscibility in synthetic tholeiitic melts and their relevance to Bushveld-complex rocks. *Canadian Mineralogist* **17**, 483–494.

Buchanan, D. L., Nolan, J., Wilkinson, N. & de Villiers, J. P. R. (1983). An experimental investigation of sulphur solubility as a function of temperature in synthetic silicate melts. *Geological Society of South Africa Special Publication* **7**, 383–391.

Chase, M. W., Jr (1998). *NIST-JANAF Thermochemical Tables*. Washington DC, USA: National Institute of Standards and Technology.

Dankwerth, P. A., Hess, P. C. & Rutherford, M. J. (1979). The solubility of sulfur in high-TiO_2 mare basalts. *Proceedings of the 10th Lunar Planetary Science Conference. Geochimica et Cosmochimica Acta Supplement* 517–530.

Darken, L. S. & Gurry, R. W. (1946). The system iron–oxygen. I. The wüstite field and related equilibria. *Journal of American Chemical Society* **67**, 1398–1412.

De Hoog, J. C. M., Mason, P. R. D. & Van Bergen, M. J. (2001). Sulfur and chalcophile elements in subduction zones: constraints from a laser ablation ICP-MS study of melt inclusions from Galunggung Volcano, Indonesia. *Geochimica et Cosmochimica Acta* **65**(18), 3147–3164.

Dixon, J. E., Clague, D. A. & Stolper, E. M. (1991). Degassing history of water, sulfur, and carbon in submarine lavas from Kilauea Volcano, Hawaii. *Journal of Geology* **99**, 371–394.

Doyle, C. D. (1988). Prediction of the activity of FeO in multicomponent magma from known values in $[SiO_2$–$KAlO_2$–$CaAl_2Si_2O_8]$–FeO liquids. *Geochimica et Cosmochimica Acta* **52**, 1827–1834.

Doyle, C. D. (1989). The effect of substitution of TiO_2 for SiO_2 on a_{FeO} in magma. *Geochimica et Cosmochimica Acta* **53**, 2631–2638.

Doyle, C. D. & Naldrett, A. J. (1986). Ideal mixing of divalent cations in mafic magma and its effect on the solution of ferrous oxide. *Geochimica et Cosmochimica Acta* **5**, 435–443.

Duffy, J. A. (1993). A review of optical basicity and its applications to oxidic systems. *Geochimica et Cosmochimica Acta* **57**, 3961–3970.

Duffy, J. A. & Ingram, M. D. (1975). Optical basicity—IV: influence of electronegativity on the Lewis basicity and solvent properties of molten oxyanion salts and glasses. *Journal of Inorganic and Nuclear Chemistry* **37**, 1203–1206.

Fincham, C. J. B. & Richardson, F. D. (1954). The behaviour of sulphur in silicate and aluminate melts. *Proceedings of the Royal Society of London, Series A* **223**, 40–62.

Flood, H., Forland, T. & Gzotheim, K. (1954). Ueber den Zusammenhang zwischen Konzentration und Aktivitäten in geschmolzenen Salzmischunge. *Zeitschrift für Anorganische Allgemeine Chemie* **276**, 290–315.

Ghiorso, M. S. & Sack, R. O. (1995). Chemical mass transfer in magmatic processes IV. A revised and internally consistent thermodynamic model for the interpolation and extrapolation of liquid–solid

equilibria in magmatic systems at elevated temperatures and pressures. *Contributions to Mineralogy and Petrology* **119**, 197–212.

Haughton, D. R., Roeder, P. L. & Skinner, B. J. (1974). Solubility of sulfur in mafic magmas. *Economic Geology* **69**, 451–467.

Jarosewich, E., Nelen, J. A. & Norberg, J. A. (1979). Electron microprobe reference samples for mineral analyses. *Smithsonian Contributions to Earth Sciences* **20**, 68–72.

Jenner, G. A. (1981). Geochemistry of high-Mg andesites from Cape Vogel, Papua New Guinea. *Chemical Geology* **33**, 307–332.

Jochum, K. P., Dingwell, D. B., Rocholl, A., Stoll, B. & Hofmann, A. W. (2000). The preparation and preliminary characterisation of eight geological MPI-DING reference glasses for in-situ microanalysis. *Geostandards Newsletter* **24**, 87–133.

Katsura, T. & Nagashima, S. (1974). Solubility of sulfur in some magmas at 1 atmosphere. *Geochimica et Cosmochimica Acta* **38**, 517–531.

Kilinc, A., Carmichael, I. S. E., Rivers, M. L. & Sack, R. O. (1983). The ferric–ferrous ratio of natural silicate liquids equilibrated in air. *Contributions to Mineralogy and Petrology* **83**, 136–140.

Kohn, S. C. (2000). The dissolution mechanisms of water in silicate melts; a synthesis of recent data. *Mineralogical Magazine* **64**, 389–408.

Kress, V. (1997). Thermochemistry of sulfide liquids. I. The system O–S Fe at 1 bar. *Contributions to Mineralogy and Petrology* **127**, 176–186.

Li, C. & Naldrett, A. J. (1993). Sulfide capacity of magma: a quantitative model and its application to the formation of sulfide ores at Sudbury, Ontario. *Economic Geology* **88**, 1253–1260.

Longhi, J. (1987). Liquidus equilibria and solid solution in the system $CaAl_2Si_2O_8$–Mg_2SiO_4–$CaSiO_3$–SiO_2 at low pressure. *American Journal of Science* **287**, 265–331.

Mathez, E. A. (1976). Sulfur solubility and magmatic sulfides in submarine basalt glass. *Journal of Geophysical Research* **81**, 4269–4276.

Mavrogenes, J. A. & O'Neill, H. S. C. (1999). The relative effects of pressure, temperature and oxygen fugacity on the solubility of sulfide in mafic magmas. *Geochimica et Cosmochimica Acta* **63**, 1173–1180.

McDonough, W. F., McCulloch, M. T. & Sun, S. S. (1985). Isotopic and geochemical systematics in Tertiary–Recent basalts from southeastern Australia and implications for the evolution of the subcontinental lithosphere. *Geochimica et Cosmochimica Acta* **49**, 2051–2067.

Métrich, N., Schiano, P., Clocchiatti, R. & Maury, R. C. (1999). Transfer of sulfur in subduction settings: an example from Batan Island (Luzon volcanic arc, Philippines). *Earth and Planetary Science Letters* **167**, 1–14.

Mysen, B. O. (1988). *Structure and Properties of Silicate Melts*. Amsterdam: Elsevier, pp. 1–354.

Nilsson, K. & Peach, C. L. (1993). Sulfur speciation, oxidation state, and sulfur concentration in backarc magmas. *Geochimica et Cosmochimica Acta* **57**, 3807–3813.

Niu, Y. & Batiza, R. (1993). Chemical variation trends at fast and slow spreading mid-ocean ridges. *Journal of Geophysical Research* **98**, 7887–7902.

Nolan, J. & Buchanan, D. L. (1984). Sulfide saturation in synthetic tholeiitic melts at 1400°C. *National Environment Research Council [Great Britain] Publication Serial* **D25**, 163–169.

O'Neill, H. St. C. & Eggins, S. M. (2002). The effect of melt composition on trace element partitioning: an experimental investigation of the activity coefficients of FeO, NiO, CoO, MoO_2 and MoO_3 in silicate melts. *Chemical Geology* (in press).

Poulson, S. R. & Ohmoto, H. (1990). An evaluation of the solubility of sulfide sulfur in silicate melts from experimental data and natural samples. *Chemical Geology* **85**, 57–75.

Roeder, P. L. (1974). Activity of iron and olivine solubility in basaltic liquids. *Earth and Planetary Science Letters* **23**, 397–410.

Seo, J. D. & Kim, S. H. (1999). The sulphide capacity of CaO–SiO_2–Al_2O_3–MgO(–FeO) smelting reduction slags. *Steel Research* **70**, 203–208.

Shima, H. & Naldrett, A. J. (1975). Solubility of sulfur in ultramafic melt and the relevance of the system Fe–S–O. *Economic Geology* **70**, 960–967.

Sosinksy, D. J. & Sommerville, I. D. (1986). The composition and temperature dependence of the sulfide capacity of metallurgical slags. *Metallurgical Transactions B* **17B**, 331–337.

Sugawara, T. (1999). Experimental techniques to minimize Fe and Na losses in one atmosphere gas mixing furnace. *Journal of Mineralogy, Petrology and Economic Geology* **94**, 425–441.

Thordarson, T., Self, S., Óskarsson, N. & Hulsebosch, T. (1996). Sulfur, chlorine, and fluorine degassing and atmospheric loading by the 1783–1784 AD Laki (Skaftár Fires) eruption in Iceland. *Bulletin of Volcanology* **58**, 205–225.

Wallace, P. & Carmichael, I. S. E. (1992). Sulfur in basaltic magmas. *Geochimica et Cosmochimica Acta* **56**, 1683–1874.

Wood, B. J. & Nicholls, J. (1978). The thermodynamic properties of reciprocal solid solutions. *Contributions to Mineralogy and Petrology* **66**, 389–400.

Young, R. W., Duffy, J. A., Hassall, G. J. & Xu, Z. (1992). Use of optical basicity concept for determining phosphorus and sulphur slag–metal partitions. *Ironmaking and Steelmaking* **19**, 201–219.